RESEARCH ARTICLE SUMMARY

MICROBIOLOGY

A bacterial phospholipid phosphatase inhibits host pyroptosis by hijacking ubiquitin
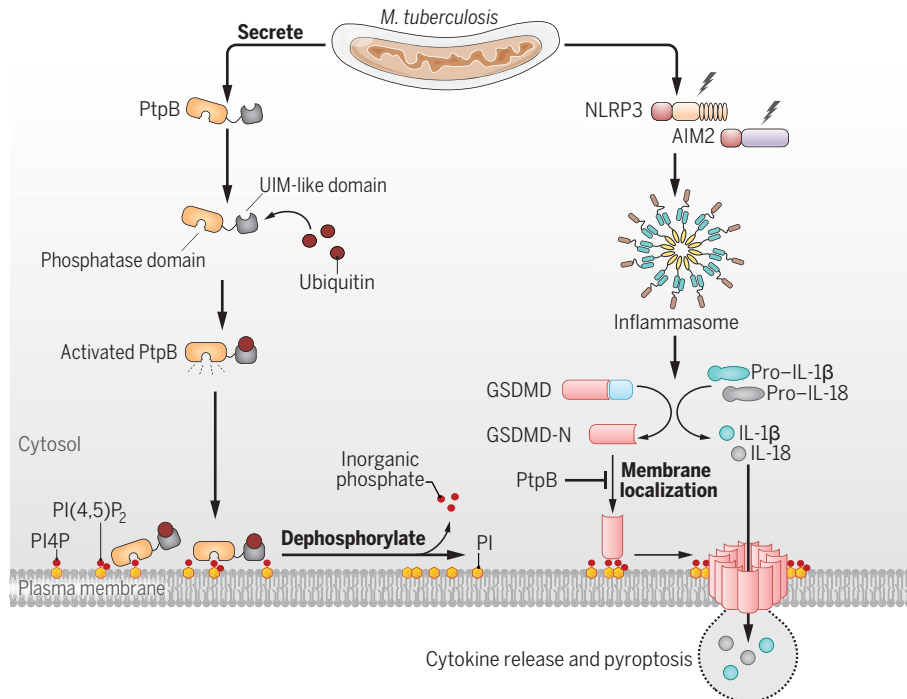
Qiyao Chai†, Shanshan Yu†, Yanzhao Zhong†, Zhe Lu, Changgen Qiu, Yang Yu, Xinwen Zhang, Yong Zhang, Zehui Lei, Lihua Qiang, Bing-Xi Li, Yu Pang, Xiao-Bo Qiu*, Jing Wang*, Cui Hua Liu*

INTRODUCTION: Pyroptosis is a proinflammatory form of programmed cell death characterized by membrane pore formation that allows the release of intracellular inflammatory mediators, a process that is elicited by the inflammasome-mediated cleavage and activation of gasdermin D (GSDMD). Growing evidence supports a critical role for pyroptosis in the control of infections by mammalian hosts, but how pathogens evade this immune response remains largely unexplored.

RATIONALE: *Mycobacterium tuberculosis* (Mtb), an ancient pathogen that causes tuberculosis (TB), has developed numerous intracellular survival strategies to evade host immunity and to drive the occurrence and development of TB. One notable feature evolved by Mtb is a set of eukaryotic-like effectors, but their host targets and regulatory roles in pathogen–host interactions remain largely unclear. In this study, we sought to identify the key pathogenic regulators of inflammasome-pyroptosis pathways from Mtb eukaryotic-like effectors, information that could improve our understanding of TB pathogenesis and provide potential targets for novel anti-TB treatment.

RESULTS: We examined the whole genome of Mtb to predict its secreted eukaryotic-like proteins possessing eukaryotic-like motifs or domains that might target host factors directly.

These Mtb effector proteins were then subjected to further experimental analyses using an inflammasome reconstitution system for screening inhibitors of inflammasome-pyroptosis pathways. Out of 201 predicted Mtb-secreted eukaryotic proteins, six Mtb proteins (Rv0153c, Rv0561c, Rv0824c, Rv0861c, Rv1515c, and Rv1679) exhibited strong inhibitory effects on both NOD-like receptor protein 3 (NLRP3) and absent in melanoma 2 (AIM2) inflammasome pathways. Among these proteins, PtpB (i.e., Rv0153c) was most abundantly secreted by Mtb during infection. We thus focused on PtpB and further confirmed its inhibitory effect on AIM2 or NLRP3 inflammasome-mediated interleukin-1β (IL-1β) secretion. Subsequent experiments demonstrated that PtpB inhibited gasdermin D (GSDMD)–dependent cytokine release and pyroptosis to promote Mtb intracellular survival in macrophages. Mechanistically, Mtb-secreted PtpB could target and dephosphorylate host plasma membrane phosphatidylinositol-4-monophosphate (PI4P) and phosphatidylinositol-(4,5)-bisphosphate [PI(4,5)P$_2$] to inhibit the membrane localization of the N-terminal cleavage fragment of GSDMD (GSDMD-N), thus preventing GSDMD-mediated immune responses. This phosphoinositide phosphatase activity requires binding of PtpB to ubiquitin. Accordingly, disrupting phospholipid phosphatase activity or the unusual ubiquitin-interacting motif (UIM)–like domain of PtpB markedly enhanced host innate immune responses and reduced intracellular pathogen survival in mice in a GSDMD-dependent manner.

CONCLUSION: We demonstrate that GSDMD-mediated pyroptosis and inflammatory cytokine release play a critical role in host anti-infection immunity, which is counteracted by Mtb effector protein PtpB. Our data reveal a role of the pathogen-derived phospholipid phosphatase in the regulation of GSDMD-dependent pyroptosis and cytokine releases, extending our understanding of the elaborate regulatory mechanism of cellular inflammasome-pyroptosis signaling pathways during pathogen infection. The present study also presents a strategy by which pathogens hijack ubiquitin to inhibit host pyroptosis by altering the phospholipid composition of the host membrane. Our discovery of the PtpB UIM-like domain, which is not homologous to any human protein, may provide potential selectivity for the development of anti-TB therapies. ∎

M. tuberculosis PtpB hijacks host ubiquitin to inhibit pyroptosis through altering host membrane phospholipid composition. *M. tuberculosis*–secreted phospholipid phosphatase PtpB is activated by interacting with host ubiquitin through a UIM-like domain, by which it dephosphorylates host plasma membrane phosphoinositides PI4P and PI(4,5)P$_2$ to inhibit the membrane targeting of GSDMD-N, thus disrupting the inflammatory cytokine release and pyroptosis upon activation of *M. tuberculosis* infection–triggered inflammasome activation in macrophages.

READ THE FULL ARTICLE AT
https://doi.org/10.1126/science.abq0132

MICROBIOLOGY

A bacterial phospholipid phosphatase inhibits host pyroptosis by hijacking ubiquitin

Qiyao Chai[1]†, Shanshan Yu[2]†, Yanzhao Zhong[1,3]†, Zhe Lu[1,3], Changgen Qiu[1,3], Yang Yu[1,3], Xinwen Zhang[1,3], Yong Zhang[1], Zehui Lei[1,3], Lihua Qiang[1,3], Bing-Xi Li[1], Yu Pang[2], Xiao-Bo Qiu[4,5]*, Jing Wang[1]*, Cui Hua Liu[1,3]*

The inflammasome-mediated cleavage of gasdermin D (GSDMD) causes pyroptosis and inflammatory cytokine release to control pathogen infection, but how pathogens evade this immune response remains largely unexplored. Here we identify the known protein phosphatase PtpB from *Mycobacterium tuberculosis* as a phospholipid phosphatase inhibiting the host inflammasome-pyroptosis pathway. Mechanistically, PtpB dephosphorylated phosphatidylinositol-4-monophosphate and phosphatidylinositol-(4,5)-bisphosphate in host cell membrane, thus disrupting the membrane localization of the cleaved GSDMD to inhibit cytokine release and pyroptosis of macrophages. Notably, this phosphatase activity requires PtpB binding to ubiquitin. Disrupting phospholipid phosphatase activity or the ubiquitin-interacting motif of PtpB enhanced host GSDMD-dependent immune responses and reduced intracellular pathogen survival. Thus, pathogens inhibit pyroptosis and counteract host immunity by altering host membrane composition.

uberculosis (TB) is a highly infectious disease caused by *Mycobacterium tuberculosis* (Mtb), which remains the leading cause of death from a single infectious agent, accounting for ~1.5 million deaths each year (*1*). This situation is being exacerbated by the emergence and spread of drug-resistant Mtb, which renders patients untreatable with currently available drugs. This is particularly troublesome as the pathogenesis of TB remains poorly understood, impeding the rational development of new anti-TB therapies (*2*). As an adaptable intracellular pathogen that coexists and coevolves within the human host, Mtb has developed numerous strategies to establish prolonged infection. One interesting feature of Mtb is a set of eukaryotic-like effectors (*3–5*), but their host cellular targets and regulatory roles in pathogen–host interactions remain largely unexplored.

The inflammasome is a multiprotein cytoplasmic complex composed of cytosolic immune sensors such as absent in melanoma 2 (AIM2) and NOD-like receptor protein 3 (NLRP3), inflammatory caspases (especially caspase-1), and apoptosis-associated speck-like

protein containing a CARD (ASC). The inflammasome mediates the secretion of inflammatory cytokines (e.g., interleukins IL-1β and IL-18) in response to infection by pathogens including Mtb (*6*). The inflammasome-mediated activation of caspase-1 leads to cleavage of gasdermin D (GSDMD), resulting in the formation of membrane pores and the induction of pyroptosis. Pyroptosis is an inflammatory form of cell death that features cytoplasmic swelling, DNA fragmentation, and leakage of cytosolic contents (*7*). Cellular membrane phospholipids, especially phosphoinositides, have recently been linked to pyroptosis and IL-1β release by macrophages (*8–10*). The distribution and abundance of phosphoinositides are regulated by cellular phosphoinositide kinases and phosphatases and may be disturbed by invading pathogens (*11*). However, it is unclear whether pathogens remodel cellular phospholipid homeostasis to manipulate host inflammasome-mediated immune responses. Here, we demonstrate that the known protein tyrosine phosphatase B (PtpB, also called Rv0153c) from Mtb alters the phospholipid composition of the host membrane by binding ubiquitin (Ub) to inhibit pyroptosis and counteract host immunity.

Results

Identification of Mtb PtpB as an inhibitor of NLRP3 and AIM2 inflammasome pathways

To predict Mtb-secreted eukaryotic-like proteins that might target host factors directly, we examined the whole genome of Mtb H37Rv and found 540 genes (accounting for ~13.8% of Mtb protein-encoding genes) that encode proteins harboring eukaryotic-like motifs or domains. Of these, 201 proteins were classified

as Mtb-secreted molecules (fig. S1A and data S1). These proteins were then subjected to an enzyme-linked immunosorbent assay (ELISA) to determine their effects on the AIM2 and NLRP3 inflammasome pathways in human embryonic kidney 293T (HEK293T) cells with a reconstituted inflammasome system (Fig. 1A). Inflammasome assembly induces autoproteolytic activation of caspase-1, which then proteolytically cleaves pro–IL-1β and GSDMD, followed by the release of mature IL-1β through cell membrane pores generated by the N-terminal cleavage fragment of GSDMD (GSDMD-N) (*7*). Our data showed that six Mtb proteins (Rv0153c, Rv0561c, Rv0824c, Rv0861c, Rv1515c, and Rv1679) exhibited strong inhibitory effects on the secretion of IL-1β from both AIM2 and NLRP3 inflammasome-reconstituted HEK293T cells [relative activation rate < 0.2; data S2]. Among these proteins, PtpB (i.e., Rv0153c) was most abundantly secreted by Mtb during infection (fig. S1B). Thus, we focused on PtpB and further confirmed its inhibitory effect on AIM2 or NLRP3 inflammasome-mediated IL-1β secretion through ELISA and immunoblotting analyses (Fig. 1B and fig. S1, C and D). Accordingly, the Mtb mutant strain with the deletion of *ptpB* (Δ*ptpB*) showed stronger pyroptosis-inducing effect in macrophages than the wild-type (WT) Mtb strain (fig. S1E and movies S1 and S2). Together, these results suggest that PtpB is an important bacterial inhibitor of the host inflammasome-pyroptosis pathway.

PtpB inhibits GSDMD-dependent cytokine release and pyroptosis

We then sought to define the specific mechanism(s) of suppression of the inflammasome pathway by Mtb PtpB. Because ASC speck formation is a marker for inflammasome assembly, we examined whether PtpB affects this process. Deletion of *ptpB* did not show significant effects on ASC speck formation in Mtb-infected macrophages (fig. S2, A and B). Proximity ligation assays confirmed that PtpB had no significant effect on the interaction between ASC and caspase-1 (fig. S2, C to E), suggesting that PtpB does not affect inflammasome assembly (*7*). PtpB also did not affect the interaction between Mtb and caspase-1 (fig. S2, F and G), indicating that certain mycobacterial proteins might interact with host caspase-1 during Mtb infection, even though this interaction is independent of PtpB. We then found that Mtb Δ*ptpB* infection resulted in lower intracellular amounts of mature IL-1β, caspase-1 (p20), and the C-terminal cleavage fragment of GSDMD (GSDMD-C) but higher supernatant amounts of these molecules compared with WT or *ptpB*-complemented (Δ*ptpB:ptpB*) Mtb strains (fig. S2H). Mature IL-1β, caspase-1 (p20), and GSDMD-C are released from the pyroptotic cells upon inflammasome activation

[1]CAS Key Laboratory of Pathogenic Microbiology and Immunology, Institute of Microbiology, Chinese Academy of Sciences, Beijing 100101, China. [2]Beijing Tuberculosis and Thoracic Tumor Research Institute, Beijing Chest Hospital, Capital Medical University, Beijing 101149, China. [3]Savaid Medical School, University of Chinese Academy of Sciences, Beijing 101408, China. [4]State Key Laboratory of Natural Medicines, China Pharmaceutical University, Nanjing, Jiangsu 211198, China. [5]Ministry of Education Key Laboratory of Cell Proliferation and Regulation Biology, College of Life Sciences, Beijing Normal University, Beijing 100875, China.
*Corresponding author. Email: xqiu@bnu.edu.cn (X.-B.Q.); wangj6@im.ac.cn (J.W.); liucuihua@im.ac.cn (C.H.L.)
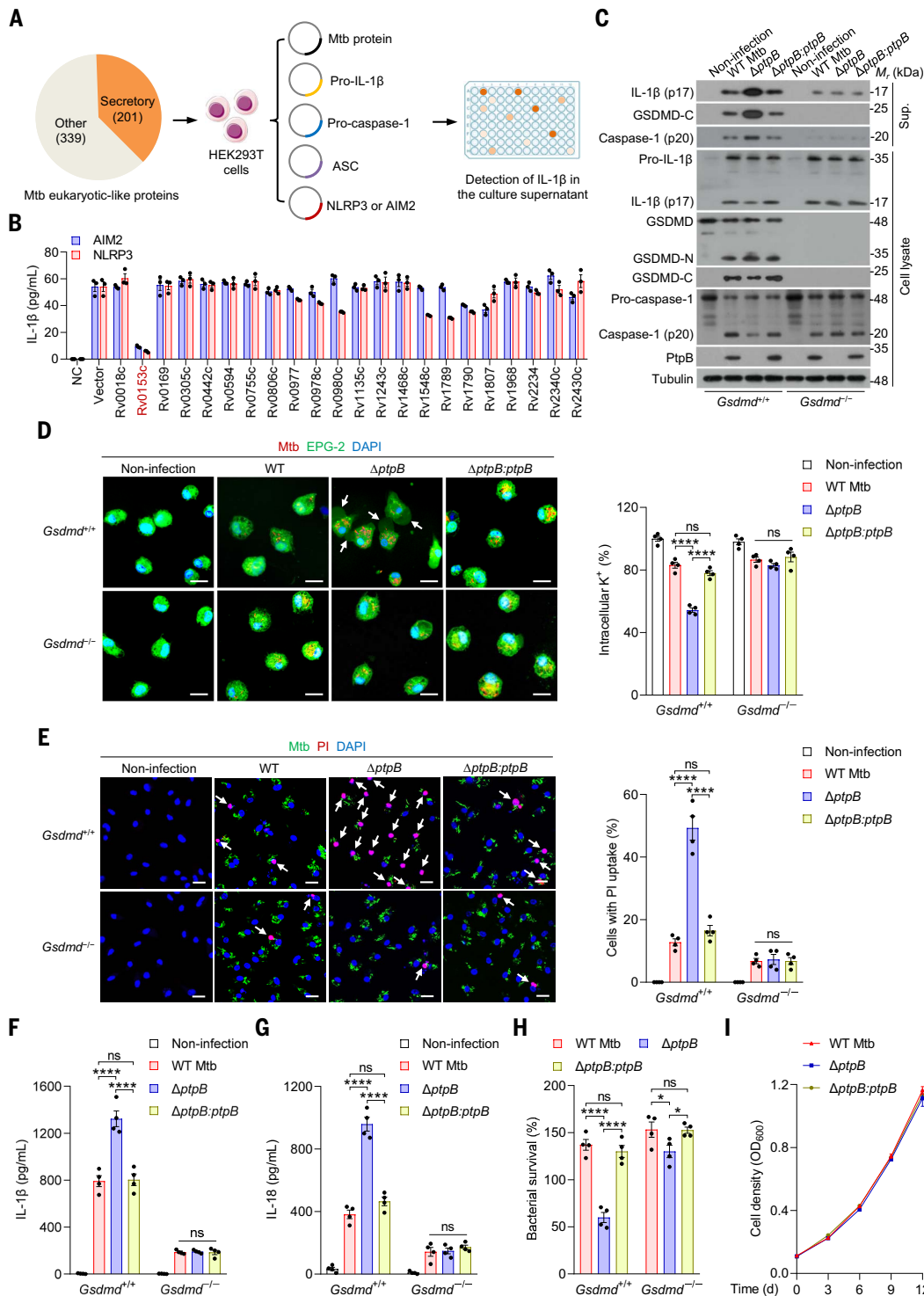†These authors contributed equally to this work.

Fig. 1. PtpB inhibits GSDMD-dependent cytokine release and pyroptosis.
(**A**) Schematic diagram of the procedure to screen Mtb inhibitors of AIM2 and NLRP3 inflammasome pathways. (**B**) Representative results of the effects of Mtb proteins on IL-1β secretion from inflammasome-reconstituted HEK293T cells. PtpB (i.e., Rv0153c) is indicated in red. NC, negative control. (**C**) Immunoblotting of the indicated proteins in the culture supernatants (Sup.) and cell lysates of $Gsdmd^{+/+}$ or $Gsdmd^{-/-}$ BMDMs. (**D**) Measurement of the K⁺ concentrations in BMDMs using Enhanced Potassium Green-2 (EPG-2). Arrows indicate the pyroptotic cells. Scale

bars, 10 μm. (**E**) Membrane integrity analysis of BMDMs. Arrows indicate propidium iodide (PI)–positive cells. Scale bars, 10 μm. (**F** and **G**) ELISA of supernatant IL-1β (F) and IL-18 (G) from BMDMs. (**H**) Intracellular survival analysis of Mtb in BMDMs. (**I**) In vitro growth kinetics of the indicated Mtb strains. For (C) to (H), cells were infected with the indicated Mtb strains for 48 hours. $P > 0.05$, not significant (ns); *$P <$ 0.05; ****$P < 0.0001$ (two-way ANOVA with Tukey's post-hoc test). Data are shown as mean ± SEM [$n = 3$ in (B) and $n = 4$ in (D) to (I)]. Data are representative of at least three independent experiments.

(*10*, *12*). Deletion of *ptpB* in Mtb increased intracellular amounts of GSDMD-N (fig. S2H), which binds to the cell membrane rather than being released into the supernatant upon inflammasome activation (*12*). Deletion of *ptpB* in Mtb decreased intracellular amounts of pro–IL-1β, probably owing to the acceleration of pro–IL-1β cleavage by enhanced inflammasome activation (fig. S2H). These observations indicate that PtpB might target GSDMD, which is required for cell membrane pore formation to allow the release of intracellular small-diameter proteins and to promote K⁺ efflux that further facilitates inflammasome activation (*10*, *13*).

Next, we obtained bone marrow–derived macrophages (BMDMs) from *Gsdmd*-deficient (*Gsdmd*⁻/⁻) and WT (*Gsdmd*⁺/⁺) mice to confirm whether GSDMD is required for PtpB-mediated inhibition of the inflammasome-pyroptosis pathway. We found that deletion of *ptpB* increased the secretion of matured IL-1β, caspase-1 (p20), and GSDMD-C in *Gsdmd*⁺/⁺ BMDMs but not in *Gsdmd*⁻/⁻ BMDMs (Fig. 1C). PtpB deletion also decreased the concentrations of K⁺ in *Gsdmd*⁺/⁺ BMDMs and induced a higher proportion of *Gsdmd*⁺/⁺ BMDMs with swelling bubbles, which are a marker of pyroptosis; these effects were abolished in *Gsdmd*⁻/⁻ BMDMs (Fig. 1D). In addition, deletion of *ptpB* in Mtb increased pyroptosis in *Gsdmd*⁺/⁺ BMDMs but not in *Gsdmd*⁻/⁻ BMDMs (Fig. 1E). Furthermore, PtpB suppressed the secretion of IL-1β and IL-18, two vital inflammatory cytokines released by macrophages upon inflammasome activation (*10*) in a GSDMD-dependent manner (Fig. 1, F and G). In contrast, PtpB inhibited the production of tumor necrosis factor α (TNF-α) and IL-6, but not IL-12 (p40) or IL-10, by macrophages in a GSDMD-independent manner (fig. S3, A to D). Accordingly, PtpB decreased mRNA levels of *Tnf* and *Il6* at various time points after Mtb infection independent of GSDMD (fig. S3, E to J), supporting the notion that PtpB is involved in Mtb suppression of several non-inflammasome immune pathways (*14*, *15*). We then examined the effects of PtpB-suppressed GSDMD-dependent inflammasome cytokine release and pyroptosis on Mtb intracellular survival and found that Mtb Δ*ptpB* exhibited a more pronounced attenuation of intracellular survival in *Gsdmd*⁺/⁺ BMDMs than in *Gsdmd*⁻/⁻ BMDMs (Fig. 1H), but Mtb Δ*ptpB* did not exhibit any growth defects in the absence of host cells (Fig. 1I). Further, we used cytokine antagonists and/or neutralizing antibodies to confirm that both GSDMD-mediated inflammatory cytokine release and pyroptosis promoted the PtpB-promoted Mtb intracellular survival (fig. S3K). We also observed that PtpB-suppressed production of TNF-α and IL-6 weakly promoted Mtb intracellular survival (fig. S3K). Next, we exogenously expressed Mtb PtpB in *Gsdmd*⁺/⁺ and *Gsdmd*⁻/⁻ BMDMs to validate the inhibitory

effect of PtpB on inflammasome pathways (fig. S4A). PtpB inhibited the GSDMD-dependent release of IL-1β and IL-18 and pyroptosis upon activation of the AIM2 and NLRP3 inflammasome pathways stimulated by poly(deoxyadenylic-deoxythymidylic) acid [poly(dA:dT)] and nigericin, respectively, in lipopolysaccharide (LPS)–primed macrophages (fig. S4, B to I). PtpB also suppressed GSDMD-independent production of TNF-α and IL-6 in LPS-stimulated macrophages (fig. S4, D and E). Taken together, these data suggest that PtpB inhibits the GSDMD-dependent inflammasome cytokine release and pyroptosis to facilitate Mtb intracellular survival, although PtpB may also impair other innate immune pathways, for example, macrophage production of TNF-α and IL-6, in a GSDMD-independent manner.

PtpB disrupts membrane localization of GSDMD-N

GSDMD-N is the functional domain of GSDMD that mediates cytokine release and pyroptosis. We examined the role of GSDMD-N in PtpB-mediated inhibition of inflammasome pathways by generating *Gsdmd*⁻/⁻ immortalized BMDMs (iBMDMs) stably expressing WT human GSDMD (hGSDMD) or hGSDMD 4A mutant, where Arg¹³⁷, Lys¹⁴⁵, Arg¹⁵¹, and Arg¹⁵³ were all mutated to Ala to inactivate GSDMD-N (Fig. 2A) (*10*). *Gsdmd*⁻/⁻ iBMDMs complemented with WT hGSDMD, but not the hGSDMD 4A mutant, restored the phenotype of macrophages infected with Mtb Δ*ptpB*, as indicated by increased amounts of supernatant IL-1β and IL-18, increased cell cytotoxicity, and reduced bacterial viability compared with the WT Mtb and Δ*ptpB:ptpB* infection groups (Fig. 2, B to E). Furthermore, expression of PtpB prominently reduced the membrane localization of GSDMD-N and cell cytotoxicity of HeLa cells (Fig. 2, F to H). Accordingly, deletion of *ptpB* markedly increased the translocation of GSDMD-N to the plasma membrane (PM) of macrophages during Mtb infection (Fig. 2I). Notably, PtpB secreted by the WT and *ptpB*-complemented strains was also detected in the PM fraction. Thus, PtpB impedes macrophage cytokine secretion and pyroptosis via GSDMD-N, whose membrane localization can be disrupted by PtpB.

PtpB impairs membrane localization of GSDMD-N depending on its lipid phosphatase activity

GSDMD-N shows a strong affinity for cell membrane lipids, particularly phosphoinositides phosphatidylinositol-4-monophosphate (PI4P) and phosphatidylinositol-(4,5)-bisphosphate [PI(4,5)P₂]. This affinity enables it to localize to the inner leaflet of the PM to form pores (*9*, *10*). Mtb PtpB is a eukaryotic-like protein tyrosine phosphatase that exhibits weak phosphoinositide phosphatase activity in vitro (*16*, *17*). The Cys¹⁶⁰→Ser (C160S) mutation abol-

ishes the phosphotyrosine and phosphoinositide phosphatase activities of PtpB, whereas the K164A mutation only eliminates the phosphotyrosine phosphatase activity of PtpB (*16*). To test whether PtpB dephosphorylates host membrane phosphoinositides to disrupt GSDMD-N membrane localization, we complemented Mtb Δ*ptpB* with the *ptpB* C160S or K164A mutant. Confocal microscopy analysis showed that PtpB and its mutants, including C160S and K164A, were secreted by Mtb and then localized to the PM of macrophages during infection (Fig. 3, A and B). PtpA, the only other protein tyrosine phosphatase identified in Mtb, did not show obvious membrane localization (*18*). Similar to the membrane lipid–binding behavior of GSDMD-N (*9*, *10*), PtpB showed strongest affinity to PI4P, followed by PI(4,5)P₂, whereas its binding affinity to sulfatides and cardiolipins was much weaker (Fig. 3C). When incubated with liposomes containing phosphatidylcholine as the skeleton lipid, PtpB and its C160S or K164A mutants were precipitated by liposomes containing 20% PI4P or PI(4,5)P₂ (Fig. 3D). Similar to *ptpB* deletion, the PtpB C160S, but not K164A, mutation increased the translocation of GSDMD-N to the PM of macrophages during Mtb infection (Fig. 3, E to G). Accordingly, the PtpB C160S mutation, but not the K164A mutation, enhanced the secretion of IL-1β and IL-18 from Mtb-infected macrophages with increased cell cytotoxicity (Fig. 3, H to J) and reduced Mtb intracellular survival, reaching a level comparable to that of Mtb Δ*ptpB* (Fig. 3K). These results demonstrate that PtpB is a membrane lipid–binding protein whose Cys¹⁶⁰-dependent lipid phosphatase activity is essential for impairing GSDMD-N membrane localization.

PtpB reduces the concentrations of plasma membrane PI4P and PI(4,5)P₂ to impair GSDMD-mediated immune functions

Next, we tested whether PtpB dephosphorylates host membrane phosphoinositides. PtpB exhibited the strongest binding to PI4P and relatively weaker affinity for PI3P, PI(3,5)P₂, and PI(4,5)P₂ in vitro (fig. S5A). We then tested whether the PtpB-induced subversion of GSDMD functions in macrophages could be restored by supplementing these phosphoinositides (fig. S5B). In both WT and *ptpB*-complemented Mtb-infected macrophages, treatment with exogenous PI4P promoted IL-1β and IL-18 secretion with increased cytotoxicity and reduced bacterial intracellular survival, reaching levels similar to those of Mtb Δ*ptpB* and Δ*ptpB:ptpB* C160S-infected macrophages (Fig. 4, A to D). Meanwhile, treatment with PI(4,5)P₂, but not PI3P or PI(3,5)P₂, partially diminished the differences among the four infection groups. PI(4,5)P₂ and its synthetic precursor PI4P are the two major phosphoinositides in the PM, whereas PI3P and PI(3,5)P₂ are primarily found
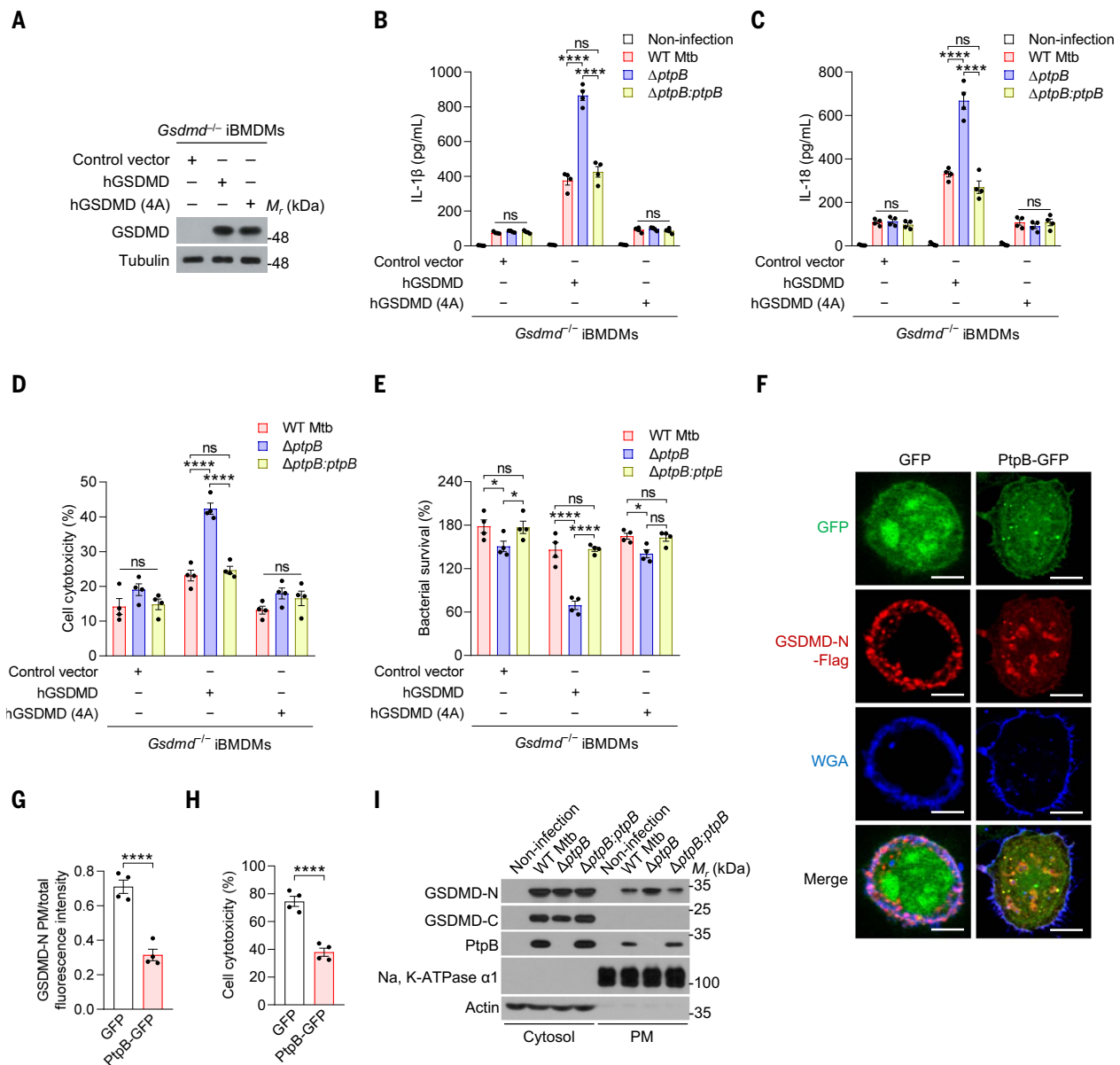
Fig. 2. PtpB disrupts membrane localization of GSDMD-N. (**A**) Immunoblotting of hGSDMD in *Gsdmd*^{−/−} iBMDMs complemented with or without WT hGSDMD or hGSDMD 4A mutant. (**B** and **C**) ELISA of supernatant IL-1β (B) and IL-18 (C) from iBMDMs treated as in (A). (**D** and **E**) Analysis for cell cytotoxicity (D) and intracellular bacterial survival (E) in iBMDMs treated as in (A). (**F**) Confocal microscopy of HeLa cells cotransfected with GSDMD-N-Flag and GFP or PtpB-GFP for 24 hours. The plasma membrane (PM) was stained with wheat germ agglutinin (WGA). Scale bars, 5 μm. (**G** and **H**) Quantitation of GSDMD-N PM/total fluorescence intensity (G) and cell cytotoxicity (H) of HeLa cells treated as in (F). (**I**) Immunoblotting of the indicated proteins in subcellular fractions of BMDMs. For (B) to (E) and (I), cells were infected with or without the indicated Mtb strains for 48 hours; $P > 0.05$, not significant (ns); $*P < 0.05$; $****P < 0.0001$ (two-way ANOVA with Tukey's post-hoc test). For (G) and (H), $****P < 0.0001$ (unpaired two-tailed *t* tests). Data are shown as mean ± SEM [$n = 4$ in (B) to (E), (G), and (H)]. Data are representative of at least three independent experiments.

in intracellular vesicles (*19*, *20*). Upon Mtb infection, PtpB markedly reduced the concentrations of PI4P and PI(4,5)P₂ in the PM, whereas it had much less effects on the concentrations of PI4P and PI(4,5)P₂ in the internal membrane (IM), which is derived from intracellular organelles (Fig. 4, E and F). Meanwhile, Mtb-secreted PtpB showed little Golgi localization in macrophages (fig. S6A). Deletion of *ptpB* had no significant effect on the Golgi pool of PI4P, Golgi

morphology, or the Golgi-mediated trafficking of Ras-related protein Rab-11A (RAB11A) and α-mannosidase II, two markers of Golgi-derived vesicles (fig. S6, B to F) (*21*, *22*). Thus, PtpB impairs GSDMD-mediated immune responses, probably by depleting host PM PI4P and PI(4,5)P₂. To verify this result, we monitored PM concentrations of PI4P and GSDMD-N during Mtb infection using immunocytochemistry (*19*). Deletion or C160S mutation of *ptpB* resulted in

comparably increased PI4P concentrations in the PM (fig. S7, A and B). In vitro analyses further confirmed the Cys¹⁶⁰-dependent phosphatase activity of PtpB toward PI4P (fig. S7C). When macrophages were treated with phenylarsine oxide (PAO) or Pik-93 to deplete cellular PI4P, the difference in membranous GSDMD-N concentrations between WT and *ΔptpB:ptpB* (C160S) strains was reduced (fig. S7, D to F). Accordingly, depletion of PM PI4P also diminished the differences
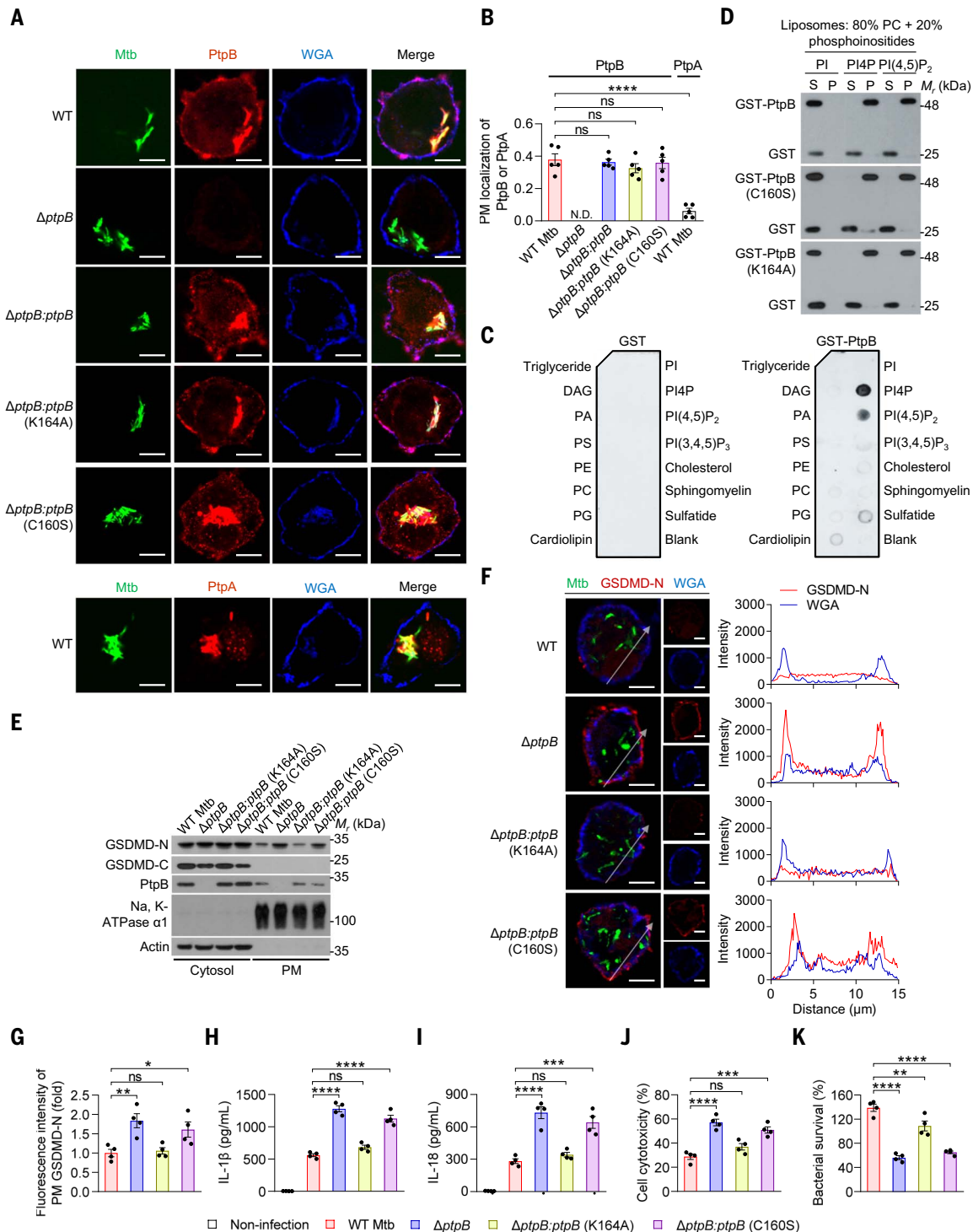
Fig. 3. PtpB impairs membrane localization of GSDMD-N depending on its lipid phosphatase activity. (**A**) Subcellular localization of PtpB and PtpA in BMDMs. The PM was stained with WGA. Scale bars, 5 μm. (**B**) Quantitation of PM PtpB and PtpA. N.D., not detectable. (**C**) Membrane lipid-binding assay of PtpB. DAG, diacylglycerol; PA, phosphatidic acid; PS, phosphatidylserine; PE, phosphatidylethanolamine; PC, phosphatidylcholine; PG, phosphatidylglycerol. (**D**) Immunoblotting of the indicated proteins in the liposome-free supernatant (S) and liposome pellet (P) after their incubation with liposomes. (**E**) Immunoblotting of the indicated proteins in subcellular fractions of BMDMs. (**F**) Confocal

microscopy of PM GSDMD-N in BMDMs with fluorescence intensity plotted along the arrows. Scale bars, 5 μm. (**G**) Quantitation of PM GSDMD-N in BMDMs. (**H** and **I**) ELISA of supernatant IL-1β (H) and IL-18 (I) from BMDMs. (**J** and **K**) Analysis for cell cytotoxicity (J) and intracellular bacterial survival (K) in BMDMs. For (A), (B), and (E) to (K), cells were infected with or without Mtb strains for 48 hours. $P > 0.05$, not significant (ns); *$P < 0.05$; **$P < 0.01$; ***$P < 0.001$; ****$P < 0.0001$ (one-way ANOVA with Dunnett's post-hoc test). Data are shown as mean ± SEM [$n = 5$ in (B) and $n = 4$ in (G) to (K)]. Data are representative of three independent experiments.
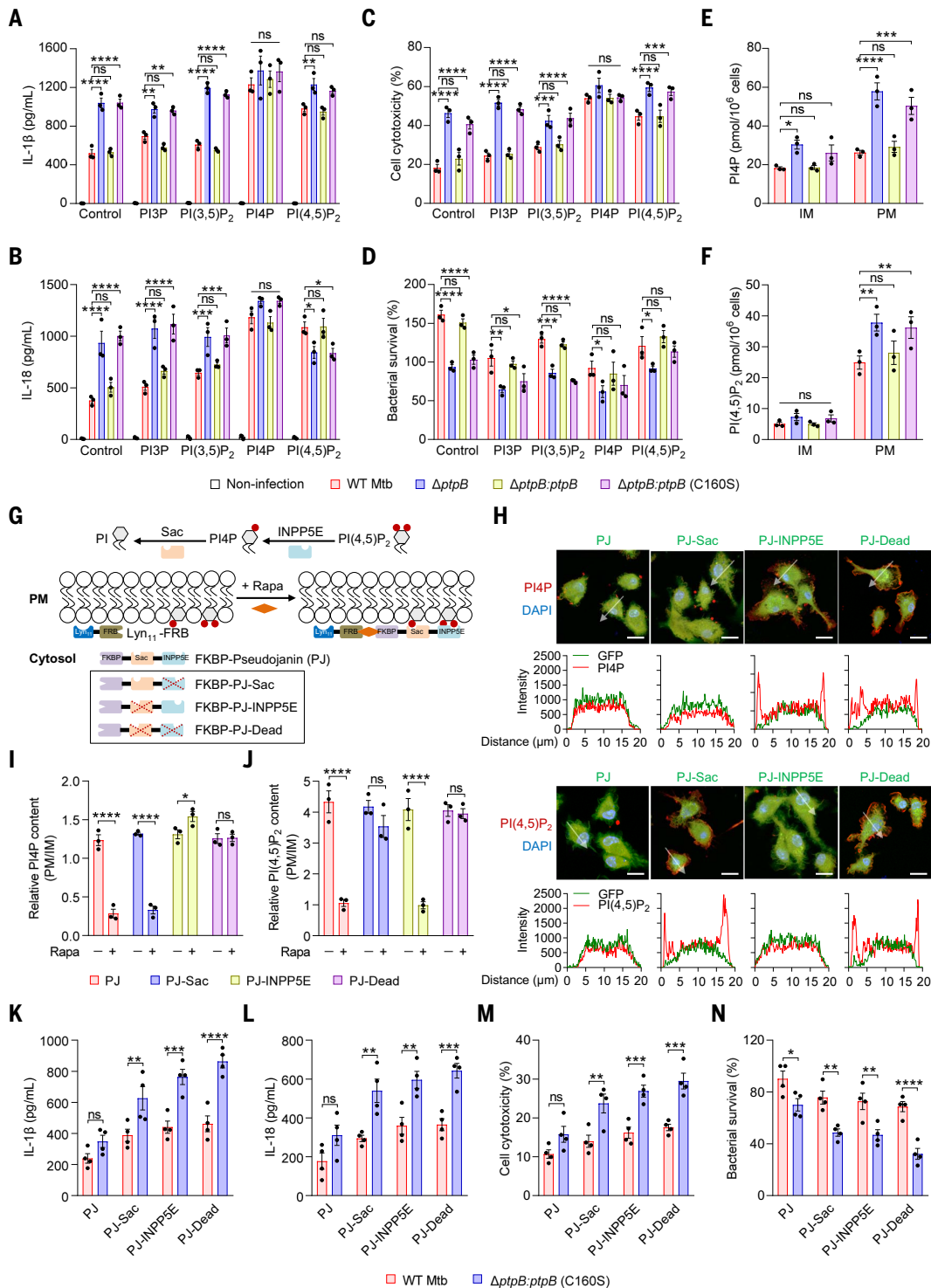
Fig. 4. PtpB reduces PM concentrations of PI4P and PI(4,5)P₂ to impair GSDMD-mediated immune functions. (**A** and **B**) ELISA of supernatant IL-1β (A) and IL-18 (B) from BMDMs. (**C** and **D**) Cell cytotoxicity (C) and intracellular bacterial survival (D) in BMDMs. (**E** and **F**) ELISA of IM- and PM-derived PI4P (E) and PI(4,5)P₂ (F) from BMDMs. (**G**) Schematic diagram of the rapamycin-induced recruitment of FKBP-PJ to PM-targeted Lyn₁₁-FRB for PI4P and PI(4,5)P₂ depletion. (**H** to **J**) Confocal microscopy (H) and ELISA of cellular PI4P (I) and PI(4,5)P₂ (J) in BMDMs after PM recruitment of PJ, PJ-Sac, PJ-INPP5E, or PJ-Dead for 10 min with 0.5 μM rapamycin. Fluorescence intensity was plotted along the arrows. Scale bars, 10 μm. (**K** and **L**) ELISA of supernatant IL-1β (K) and IL-18 (L) from BMDMs. (**M** and **N**) Cell cytotoxicity (M) and intracellular bacterial survival (N) in BMDMs. For (A) to (F), cells were infected with Mtb strains for 24 hours with or without the treatment of phosphoinositides (10 μM). For (K) to (N), cells were treated with 0.5 μM rapamycin for 10 min before infection with Mtb for 8 hours. P > 0.05, not significant (ns); *P < 0.05; **P < 0.01; ***P < 0.001; ****P < 0.0001 (two-way ANOVA with Dunnett's post-hoc test). Data are shown as mean ± SEM [n = 3 in (A) to (F), (I), and (J), and n = 4 in (K) to (N)]. Data are representative of at least three independent experiments.

in IL-1β and IL-18 release, cell cytotoxicity, and bacterial survival in macrophages between the WT Mtb and Mtb Δ*ptpB:ptpB* C160S infection groups (fig. S7, G to J). Likewise, the C160S mutation abolished the PtpB-mediated reduction in PM PI(4,5)P$_2$ concentrations in Mtb-infected macrophages (fig. S8, A and B). The depletion of cellular PI(4,5)P$_2$ using ionomycin partially diminished the differences in IL-1β and IL-18 release, cell cytotoxicity, and bacterial intracellular survival between WT Mtb and Mtb Δ*ptpB:ptpB* C160S infection groups (fig. S8, C to F). To exclude the possibility that the inhibitory effect of PtpB on GSDMD functions might be due to its pleiotropic phosphatase activity in depleting both PM and IM PI4P and PI(4,5)P$_2$, and to avoid the undesired effects of PAO, Pik-93, and ionomycin on other phosphoinositides, we turned to a rapamycin-inducible PM phosphoinositide depletion approach using two constructs including PM-targeted Lyn$_{11}$-FRB and cytosolic FKBP-Pseudojanin (PJ), which dephosphorylates PI4P and PI(4,5)P$_2$ (Fig. 4G; see table S1 for details) (*23*). The recruitment of PJ to the PM decreased PM PI4P and PI(4,5)P$_2$ concentrations in response to rapamycin, while PJ-Sac (which dephosphorylates PI4P) and PJ-INPP5E [which dephosphorylates PI(4,5)P$_2$], but not PJ-Dead [which dephosphorylates neither PI4P nor PI(4,5)P$_2$], selectively reduced PM PI4P and PI(4,5)P$_2$ concentrations, respectively (Fig. 4, H to J). These results demonstrate the feasibility of this approach in depriving PM PI4P and/or PI(4,5)P$_2$ in macrophages. We then found that the PM recruitment of PJ, but not of PJ-Dead, partially reduced the amounts of membranous GSDMD-N (L192D) (which retards pyroptosis to enable monitoring) (*10*), concurrent with decreased cell cytotoxicity (fig. S9). Meanwhile, the PM recruitment of either PJ-Sac or PJ-INPP5E alone had little, if any, effect on the membranous GSDMD-N (L192D) concentrations and cell cytotoxicity (fig. S9). These data indicate that the PM PI4P and PI(4,5)P$_2$ have synergistic effects on PM localization of GSDMD-N. The remaining undissociated PM GSDMD-N is probably due to their stable membrane insertion after oligomerization with drastic conformational changes (*10*). Finally, the PJ-induced depletion of PM PI4P and PI(4,5)P$_2$ significantly reduced the differences in IL-1β and IL-18 release, cell cytotoxicity, and bacterial survival in macrophages between the WT Mtb and Mtb Δ*ptpB:ptpB* C160S infection groups (Fig. 4, K to N). Together, these findings suggest that PtpB can dephosphorylate and therefore reduce the PM concentrations of PI4P and PI(4,5)P$_2$ to impair GSDMD-mediated immune responses.

Ubiquitin binding is required for PtpB to disrupt GSDMD-mediated immune responses

We next investigated how PtpB efficiently reduces host PM PI4P and PI(4,5)P$_2$ abundance to impair GSDMD function, given that its lipid phosphatase activity is not easily detectable in vitro (fig. S7C) (*16*, *24*). The structure of PtpB features a buried active site with a phosphate-binding loop (or P-loop; Cys^{160}-X$_5$-Arg^{166}) covered by a flexible two-helix "lid," suggesting that the phosphatase activity of PtpB is regulable in vivo (*25*). We have previously shown that another Mtb protein tyrosine phosphatase, PtpA, can exploit host Ub (*5*). Structure-based analysis of the interaction between PtpB and Ub revealed that PtpB harbors a Ub-interacting motif (UIM)–like region with a hydrophobic surface including three key UIM residues (Ala^{240}–Ala^{242}) on an α helix (i.e., helix α9) that potentially bind the Ile^{44} residue in Ub (Fig. 5A) (*26*). To confirm whether this UIM-like region mediates the interaction between PtpB and Ub, we generated a PtpB mutant with Ala^{240}–Ala^{242} to Glu mutations (PtpB 3E), which predictably disrupts the hydrophobic surface but reserves helix α9 (fig. S10, A and B). PtpB bound to Ub directly in vitro and also interacted with Ub in the cells, whereas the PtpB 3E (but not C160S) or Ub I44A mutation subverted their interaction (Fig. 5B and fig. S10C). Moreover, PtpB could only interact with mono-Ub, not poly-Ub chains (fig. S10, D and E). Helix α9 of PtpB is adjacent to α8, which constitutes a structurally dynamic lid together with α7. Thus, the binding of Ub to the UIM-like region might induce a conformational change in PtpB to expose the P-loop and promote its substrate turnover (*25*). As expected, Ub increased the catalytic efficiency of WT PtpB, but not its 3E mutant, toward PI4P and the phosphotyrosine peptides of the epidermal growth factor receptor (EGFR) or insulin-like growth factor 1 receptor (IGF1R) (Fig. 5C and fig. S10F). However, Ub-like proteins, including neural precursor cell–expressed developmentally down-regulated protein 8 (NEDD8), human leukocyte antigen F-associated transcript 10 (FAT10), interferon-stimulated gene 15 (ISG15), small ubiquitin-related modifier 1 (SUMO1), ubiquitin-fold modifier 1 (UFM1), autophagy-related protein 12 (ATG12), autophagy-related protein 8 (ATG8), and ubiquitin-related modifier 1 (URM1), did not interact with PtpB and thus had no effects on PtpB activity (fig. S10G). During infection, the PtpB 3E mutation did not affect PtpB secretion by Mtb or its PM localization but did markedly increase the abundance of PI4P, PI(4,5)P$_2$, and GSDMD-N in the PM of the infected macrophages (Fig. 5, D to F, and fig. S10, H and I). Likewise, both the 3E and C160S mutation attenuated the PtpB-induced inhibition of GSDMD-N membrane localization and cytotoxicity in HeLa cells (fig. S11). In vitro kinetic analyses further supported that the addition of Ub markedly increases the catalytic efficiency of WT PtpB, but not of its C160S or 3E mutant, toward PI4P (Fig. 5G and fig. S12). However, the effect of Ub was relatively weaker for PI(3,5)P$_2$ and PI(4,5)P$_2$ and negligible for PI3P and PI5P. Hence, Ub binding appears to be critical for PtpB to dephosphorylate host phosphoinositides to inhibit GSDMD-mediated immune responses. To further confirm this hypothesis, we infected *Gsdmd*$^{+/+}$ or *Gsdmd*$^{-/-}$ BMDMs with each of the aforementioned Mtb *ptpB* variant strains. Similar to Mtb Δ*ptpB* and Δ*ptpB:ptpB* C160S strains, Mtb Δ*ptpB:ptpB* 3E enhanced secretion of IL-1β and IL-18, increased cell cytotoxicity, and reduced intracellular viability in *Gsdmd*$^{+/+}$ BMDMs but not *Gsdmd*$^{-/-}$ BMDMs (Fig. 5, H to K). These data demonstrate that Ub binding is required for PtpB to disrupt the GSDMD-dependent immune responses in macrophages during Mtb infection.

PtpB–ubiquitin interaction is required for Mtb to evade host GSDMD-dependent immunity

We then sought to determine the role of PtpB in GSDMD-dependent host immunity during Mtb infection in a mouse model. Similar to *ptpB* deletion, *ptpB* C160S and 3E mutations markedly reduced Mtb-induced inflammatory infiltration in the lungs and livers of *Gsdmd*$^{+/+}$ mice (Fig. 6, A and B, and fig. S13, A and B). However, each Mtb *ptpB* variant strain caused comparable histopathological changes in *Gsdmd*$^{-/-}$ mice. Notably, *Gsdmd*$^{-/-}$ mice showed diffused cellular infiltration rather than the typical granulomatous lesions in the lungs (Fig. 6A), which supports the recently proposed notion that the activation of inflammasome pathways is critical for inflammatory cytokine–mediated granuloma formation (*27*). In *Gsdmd*$^{+/+}$ mice, *ptpB*-deleted or *ptpB*-mutated Mtb strains induced comparable numbers of, but much smaller, lung granulomatous lesions than those caused by *ptpB*-sufficient strains at 3 weeks after infection (Fig. 6A). Accordingly, deletion or mutation of *ptpB* in Mtb comparably reduced bacterial loads both in the lungs and spleens of mice at 3 and 12 weeks after infection in a *Gsdmd*-dependent manner (Fig. 6, C and D, and fig. S13, C and D). Furthermore, deletion or mutation of *ptpB* in Mtb led to significantly increased amounts of IL-1β and IL-18 in bronchoalveolar lavage fluid (BALF) obtained from *Gsdmd*$^{+/+}$ mice at 3 weeks after infection (Fig. 6E). In addition, *ptpB*-deleted or *ptpB*-mutated Mtb strains caused increased amounts of interferon-γ (IFN-γ) in both BALF and lungs of *Gsdmd*$^{+/+}$ mice (Fig. 6E). Interestingly, the amounts of these inflammatory cytokines in *Gsdmd*$^{+/+}$ mice caused by *ptpB*-deleted or *ptpB*-mutated Mtb strains decreased slightly at 12 weeks after infection, whereas the *ptpB*-sufficient strain-induced inflammatory cytokines in *Gsdmd*$^{+/+}$ mice drastically increased at 12 weeks after infection (Fig. 6E). Moreover, the deletion of
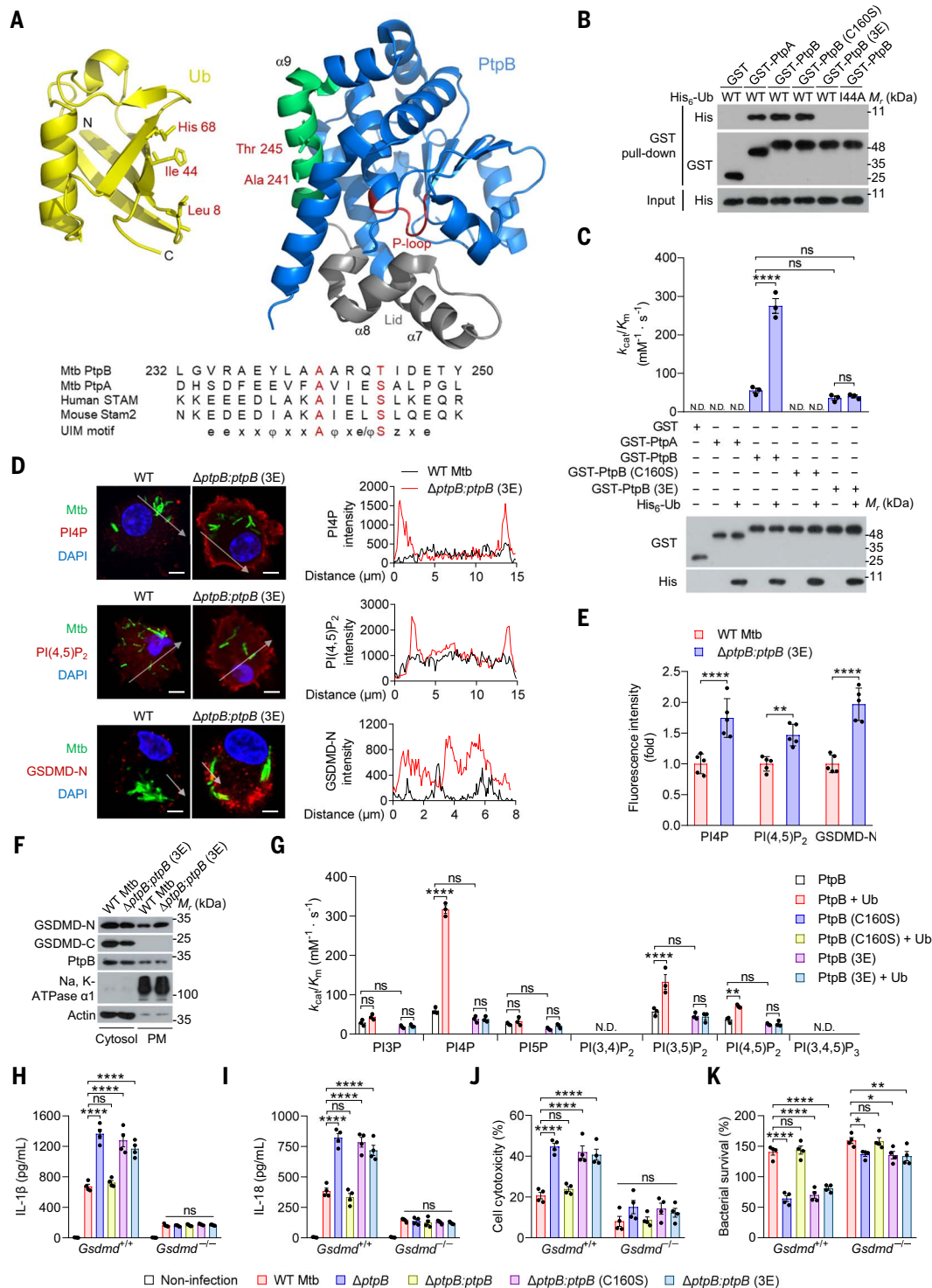
Fig. 5. Ubiquitin binding is required for PtpB to disrupt GSDMD-mediated immune responses. (**A**) Interfaces between PtpB and ubiquitin. Lower panel, alignment of PtpB UIM-like region with the related region of the indicated proteins. Single-letter abbreviations for the amino acid residues are as follows: A, Ala; C, Cys; D, Asp; E, Glu; F, Phe; G, Gly; H, His; I, Ile; K, Lys; L, Leu; M, Met; N, Asn; P, Pro; Q, Gln; R, Arg; S, Ser; T, Thr; V, Val; W, Trp; and Y, Tyr. (**B**) GST pull-down analysis for the PtpB-ubiquitin interaction. (**C**) PI4P phosphatase activity and immunoblotting of PtpB and its mutants with or without ubiquitin. N.D., not detectable. (**D** and **E**) Confocal microscopy (D) and quantitation (E) of PM PI4P, PI(4,5)P$_2$, and GSDMD-N in BMDMs. Fluorescence intensity was plotted along the arrows. Scale bars, 5 μm.

(**F**) Immunoblotting of the indicated proteins in subcellular fractions of BMDMs. (**G**) Phosphoinositide phosphatase activity analysis of PtpB and its mutants. N.D., not detectable. (**H** and **I**) ELISA of supernatant IL-1β (H) and IL-18 (I) from BMDMs. (**J** and **K**) Analysis for cell cytotoxicity (J) and intracellular bacterial survival (K) in BMDMs. Cells were infected with Mtb strains for 48 hours in (D) to (F), and (H) to (K). $P > 0.05$, not significant (ns); *$P < 0.05$; **$P < 0.01$; ****$P < 0.0001$. One-way ANOVA with Tukey's post-hoc test for (C); two-way ANOVA with Tukey's post-hoc test for (E) and (G), and with Dunnett's post-hoc test for (H) to (K). Data are shown as mean ± SEM [$n = 3$ in (C) and (G), $n = 5$ in (E), and $n = 4$ in (H) to (K)]. Data are representative of at least three independent experiments.

Fig. 6. PtpB-ubiquitin interaction is required by Mtb to evade host GSDMD-dependent immunity.
(**A**) Histopathology of lung sections from $Gsdmd^{+/+}$ or $Gsdmd^{-/-}$ mice infected with or without the indicated Mtb strains by aerosol (~ 100 CFUs) for 0 to 12 weeks. Arrows indicate foci of cellular infiltration. Scale bars, 200 μm. (**B**) Quantitation of inflammatory areas in the lungs of mice infected with Mtb as in (A). (**C** and **D**) Bacterial CFUs in lungs (C) and spleens (D) of mice infected with Mtb as in (A). N.D., not detectable. (**E**) ELISA of cytokines (IL-1β, IL-18, and IFN-γ) in bronchoalveolar lavage fluid (BALF; upper) or lung homogenates (lower) of mice infected with Mtb as in (A). (**F**) TUNEL staining of lung sections from $Gsdmd^{+/+}$ or $Gsdmd^{-/-}$ mice at 3 weeks after infection with Mtb. Scale bars, 100 μm. (**G**) Quantitation of TUNEL-positive cells in lungs of mice infected with Mtb as in (F). $P > 0.05$, not significant (ns); *$P < 0.05$; **$P < 0.01$; ***$P < 0.001$; ****$P < 0.0001$ (two-way ANOVA with Dunnett's post-hoc test). Data are shown as mean ± SEM of $n = 5$. Data are representative of at least three independent experiments.
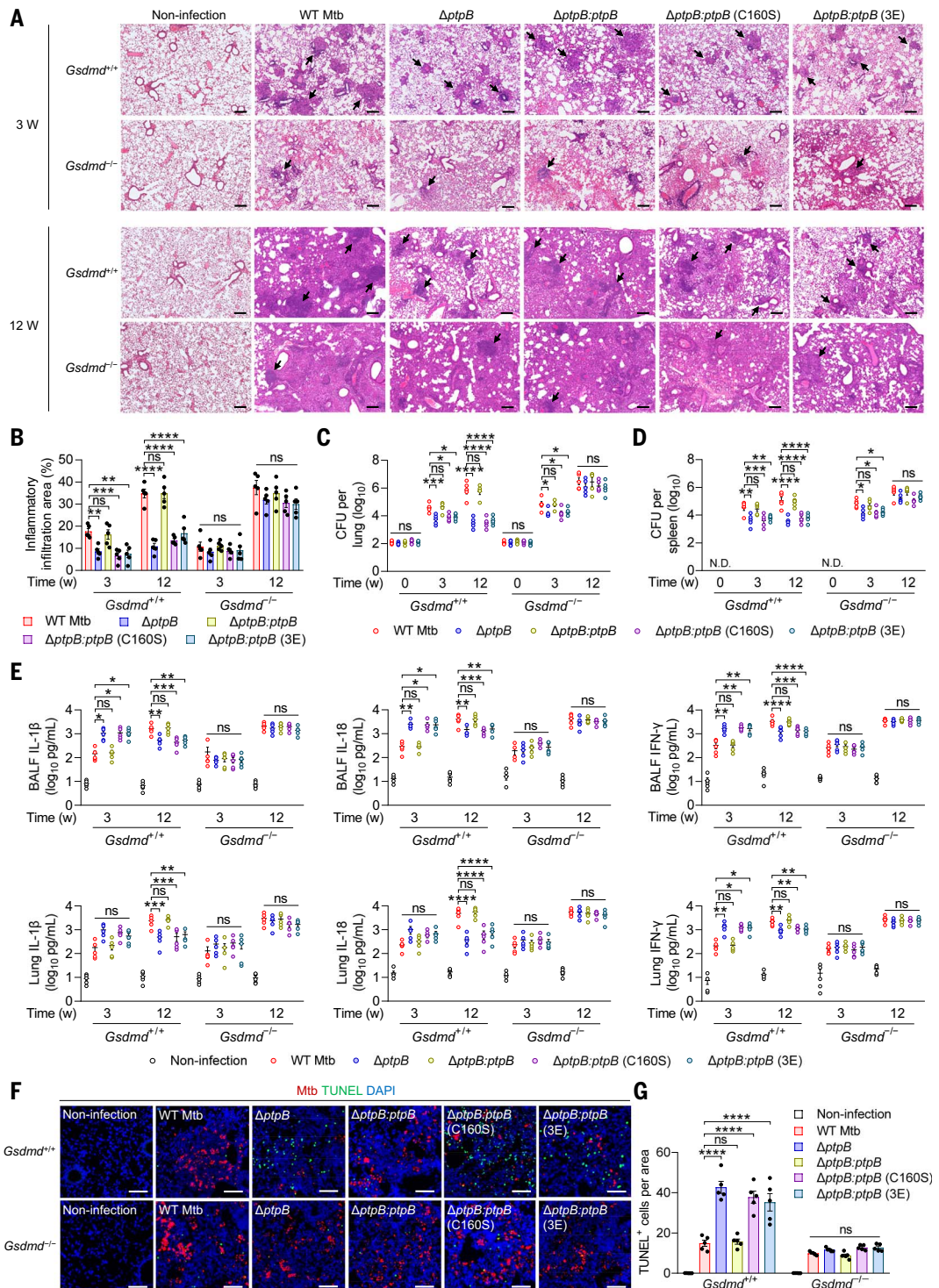
$Gsdmd$ in mice abolished the differences in cytokine amounts in the BALF and lungs of mice infected with different Mtb strains (Fig. 6E). Accordingly, the $ptpB$-deleted or $ptpB$-mutated Mtb strain, but not the $ptpB$-sufficient strain, caused higher mRNA levels of $Il1b$, $Il18$, and $Ifng$ in $Gsdmd^{-/-}$ mice than those in $Gsdmd^{+/+}$ mice at 12 weeks after infection (fig. S13E). The elevated amounts of inflammatory cytokines in $Gsdmd^{-/-}$

mice at 12 weeks after infection are probably due to excessive bacterial loads of different Mtb strains. Finally, compared with the WT and $ptpB$-complemented strains, $ptpB$-deleted and $ptpB$-mutated Mtb strains induced more TUNEL-positive cells with decreased bacterial staining in mouse lungs in a $Gsdmd$-dependent manner (Fig. 6, F and G), indicating enhanced host GSDMD-mediated pyroptosis and anti-

bacterial immunity (28). Taken together, our results suggest that PtpB is required by Mtb to evade host GSDMD-mediated immune responses, depending on the Ub-activated lipid phosphatase activity of PtpB.

Discussion

Mtb represents an extraordinary paradigm of intracellular pathogens that deliver multiple

effectors into host cells for immune evasion (*3*, *29*). Our data indicate that nearly one-seventh of Mtb genes encode proteins containing eukaryotic-like functional domains or motifs, demonstrating the astute adaptation of Mtb to its human host after eons of coevolution (*30*). Among these potential pathogenic factors, we identified PtpB as a potent inhibitor of host pyroptosis that subverts GSDMD functions to facilitate Mtb intracellular survival. Recently, the emerging role of pyroptosis in host anti-infection and tumor immunity has attracted increasing attention, and gasdermin family members have been considered as key immune factors targeted by pathogens such as *Shigella* (*31–34*). However, their exact roles in TB pathogenesis remain unclear. We showed that GSDMD-mediated pyroptosis and inflammatory cytokine release play critical roles in host anti-infection immunity, which is counteracted by the Mtb effector protein PtpB. When Mtb lacks functional PtpB, it cannot counteract host GSDMD-mediated immunity, meaning that GSDMD could confer prompt and robust host protective immune responses against infection in the early stage of infection, thus restricting bacterial survival to avoid host excessive pathogenic inflammatory responses at a later stage. Therefore, PtpB may be an attractive target for improving the immune efficacy of Bacille Calmette-Guérin, the only licensed TB vaccine whose genome harbors a PtpB-encoding gene identical to that of Mtb (*35*).

Disordered cellular lipid metabolic homeostasis has recently been linked to TB pathogenesis but is not fully understood (*36–38*). Phosphoinositides are a group of cellular membrane lipids involved in pyroptosis (*10*, *11*). However, whether and how they are regulated by invading pathogens during this immune process remains largely unclear. Mtb PtpB has been linked to host cell death and innate immune pathways (*14*, *15*). Here, we showed that PtpB can dephosphorylate host cell membrane PI4P and PI(4,5)P$_2$ upon activation by Ub to efficiently suppress GSDMD-mediated inflammatory responses. Our data reveal a regulatory role of pathogen-derived phospholipid phosphatase in the GSDMD-dependent pyroptosis and cytokine release, extending our understanding of the elaborate regulatory mechanism of cellular inflammasome signaling pathways during pathogen infection.

The mammalian Ub system subtly modulates diverse immune responses by controlling protein ubiquitination; thus, it is a common target of effectors from pathogens, including Mtb (*4*, *39*). In this study, we revealed that Mtb-secreted PtpB localizes to the host cell membrane, where it efficiently dephosphorylates phosphoinositides upon hydrophobic interaction with cytosolic Ub to impair GSDMD-mediated immunity. A structural study revealed

that PtpB harbors a buried phosphatase active site covered by a dynamic lid (*25*). Therefore, the activation of PtpB through Ub binding suggests a delicate strategy by which Mtb precisely controls the catalytic activity of PtpB to counteract the host immune system. Our data elucidate a strategy by which pathogens hijack Ub to inhibit host pyroptosis by altering the phospholipid composition of the host membrane. Our discovery of the PtpB UIM-like domain, which is not homologous to any human protein, may provide potential selectivity for the development of anti-TB therapies.

Materials and methods
Bacterial strains and plasmids

Escherichia coli DH5α were grown in flasks using LB medium for genetic manipulations. Mtb H37Rv strains were grown in Middlebrook 7H9 broth (7H9) supplemented with 10% oleic acid-albumin-dextrose-catalase (OADC) and 0.05% Tween-80, or on Middlebrook 7H10 agar supplemented with 10% OADC. Mtb with deletion of *ptpB* (NCBI gene ID: 886842; Δ*ptpB*) was created using the pJV53 system (*40*). pMV306 plasmid (kindly provided by W. R. Jacobs, Albert Einstein College of Medicine, Yeshiva University) was used to complement the strain Mtb Δ*ptpB* with WT *ptpB* or create variant strains Mtb Δ*ptpB:ptpB* (C160S) and Mtb Δ*ptpB:ptpB* (3E). pSC300 plasmid was used for expression of Mtb proteins with C-terminal green fluorescent protein (GFP) in Mtb. The mammalian expression plasmids for hemagglutinin (HA)–tagged ubiquitin (Ub); Myc-tagged human AIM2, ASC, and IL-1β; and Flag-tagged human caspase-1, NLRP3, and GSDMD-N were kindly provided by F. Shao (National Institute of Biological Sciences, Beijing). HA-tagged K6 only, K11 only, K27 only, K29 only, K33 only, K48 only, and K63 only Ub were kind gifts from L. Zhang (Beijing Institute of Lifeomics, Beijing). The full-length cDNA of PtpB was amplified from Mtb H37Rv genomic DNA, and those of human GSDMD, NEDD8, and ATG12 were amplified from U937 cDNA. Nucleotide sequences for expressing OSH2-PH×2, Lyn$_{11}$-FRB, and FKBP-Pseudojanin (PJ) were designed on the basis of previous studies (*23*, *41*) and were synthesized by GenScript Biotechnology (Nanjing) (see table S1 for details). The sequence information of these recombinant genes (GenBank accession numbers OP056760, OP056761, and OP056762, respectively) has been deposited at GenBank (https://www.ncbi.nlm.nih.gov/genbank/) and is publicly available as of the date of publication. For expression in mammalian cells, genes were cloned into the vector pcDNA6A, pEGFP-N1, pEGFP-C1, or pmCherry-N1. Prokaryotic expression plasmids were constructed by inserting the genes into the vector pGEX-6p-1 or pET30a. Point mutations were generated by using Fast Mutagenesis Kit V2 (Vazyme Bio-

tech). All of the strains, plasmids, and primers used in this study are detailed in table S1.

Antibodies and reagents

Rabbit antibodies against Mtb PtpB or PtpA were prepared and purified as described previously (*5*, *18*). Briefly, a total of 5 mg of glutathione *S*-transferase (GST)–PtpB or GST-PtpA fusion proteins were purified and solubilized in Freund's complete adjuvant for injection into rabbits. The antibodies specific to PtpB or PtpA were isolated by passaging the immunized rabbit serum on protein A agarose (Santa Cruz). All of the antibodies used in this study are listed in table S2. Phosphoinositides including PI3P, PI4P, PI5P, PI(3,4)P$_2$, PI(3,5)P$_2$, PI(4,5)P$_2$, and PI(3,4,5)P$_3$ were purchased from Echelon Biosciences (Cat# P-3016, P-4016, P-5016, P-3416, P-3516, P-4516, and P-3916, respectively). Phosphotyrosine peptides pTyr-EGFR (DADE-pY-LIPQQG) and pTyr-IGF1R (TRDI-pY-ETDYYRK) were synthesized by GenScript Biotechnology (Nanjing). Lipopolysaccharide from *E. coli* 0111:B4 (Cat# tlrl-eblps), nigericin (Cat# tlrl-nig), and poly(dA:dT) (Cat# tlrl-patc) were purchased from InvivoGen. Pik-93 (Cat# S1489) and rapamycin (Cat# S1039) were purchased from Selleck. Phenylarsine Oxide (PAO) was purchased from Shanghai Yuanye Bio-Technology (Cat# Y17991). Ionomycin was purchased from Abcam (Cat# ab120116). Recombinant mouse IL-1 receptor antagonist (IL-1RA; Cat# 769702) and IL-18 binding protein (IL-18BP; Cat# HY-P75841) were purchased from BioLegend and MedChemExpress, respectively. Human Ub$_4$ WT Chains (K48-linked), Human Ub$_4$ WT Chains (K63-linked), and Human Ub$_4$ WT Chains (M1-linked) were purchased from Boston Biochem (Cat# UC-210B, UC-310B, and UC-710B, respectively).

Cell lines

HEK293T (ATCC, Cat# CRL-3216) and HeLa (ATCC, Cat# CCL-2) cells were obtained from the American Type Culture Collection (ATCC). Immortalized murine bone marrow–derived macrophages (iBMDMs) derived from *Gsdmd*$^{-/-}$ mice on C57BL/6 genetic background were kindly provided by F. Shao (National Institute of Biological Sciences, Beijing, China). HEK293T, HeLa, and iBMDMs were cultured in Dulbecco's modified Eagle's medium (DMEM; Gibco) with 10% fetal bovine serum (FBS; Gemini Bioproducts). Cells were cultured at 37°C in a 5% CO$_2$ incubator.

Mice

WT (*Gsdmd*$^{+/+}$) C57BL/6 mice were purchased from Beijing Vital River Laboratory Animal Technology. *Gsdmd*-deficient (*Gsdmd*$^{-/-}$) mice on C57BL/6 genetic background were a kind gift of F. Shao (National Institute of Biological Sciences, Beijing, China). *Gsdmd*$^{-/-}$ mice were bred with C57BL/6 mice to obtain *Gsdmd*$^{+/-}$

heterozygotes. $Gsdmd^{-/-}$ mice and littermate controls obtained from heterozygote crosses were used for all experiments. All mice were housed in a specific pathogen–free (SPF) facility according to standard humane animal husbandry protocols, which were approved by the animal care and use committee of the Institute of Microbiology (Chinese Academy of Sciences).

Prediction of Mtb-secreted eukaryotic-like proteins

The entire genome sequence and information of Mtb H37Rv were obtained from National Center for Biotechnology Information (NCBI; RefSeq: NC_000962.3). Each corresponding sequence of encoded proteins was downloaded from UniProt database (https://www.uniprot.org/proteomes/UP000001584/), and their harboring functional domains were predicted with the SMART database (http://smart.embl-heidelberg.de/). Each protein-encoding gene was then functionally classified using the PANTHER database (http://www.pantherdb.org/). Mtb proteins that contain one or more eukaryotic-like domains or motifs identified from Effective DB (https://effectivedb.org/) were considered as eukaryotic-like proteins. The subcellular localization of each Mtb protein was annotated according to the published articles (see data S1). Circos plot that depicts Mtb genome features was generated with Circos 0.69-8 (http://www.circos.ca/soft-ware/) using the information of Mtb H37Rv genome location from Mycobrowser (https://mycobrowser.epfl.ch/).

Screening for Mtb inhibitors of inflammasome pathway

The full-length cDNAs of 201 Mtb proteins were amplified from Mtb H37Rv genomic DNA (see data S3) and were cloned into the vector p3×Flag-CMV-14 (Sigma-Aldrich). HEK293T cells in 24-well cluster plates were transfected with pCS2-Myc-ASC (50 ng), pCS2-Flag-caspase-1 (50 ng), and pCS2-Myc-IL-1β (325 ng) in combination with pCS2-Myc-AIM2 or pCS2-Flag-NLRP3 (75 ng), and a Mtb protein expression plasmid or the control empty plasmid (250 ng) using Hieff Trans Liposomal Transfection Reagent (Yeasen). At 24 hours after transfection, cell-free supernatants were collected, and IL-1β concentrations were measured by ELISA. For inflammasome reconstitution assay, cells were collected and lysed for immunoblotting with the indicated antibodies to analyze the expression of each transfected plasmid.

In vitro growth kinetics of Mtb strains

To determine the in vitro growth kinetics, Mtb strains were inoculated into Middlebrook 7H9 broth supplemented with 10% OADC and 0.05% Tween-80 at OD_{600} of ~0.1 and cultivated at 37°C. Growth of the cultures was followed by measuring the light absorbance at 600 nm every 3 days.

Preparation of BMDMs

BMDMs were collected from tibiae and femurs of 6-week-old male mice. After lysis of red blood cells, BMDMs were cultured in DMEM supplemented with 10% FBS, 1% penicillin-streptomycin solution (Caisson) and murine macrophage colony-stimulating factor (Pepro Tech) for 4 to 6 days. For each experimental design, at least two $Gsdmd^{-/-}$ mice and littermate controls were chosen to prepare the BMDM cells for analysis.

Macrophage infection and colony-forming unit counting

For macrophage infection, Mtb in Middle brook 7H9 medium (BD Biosciences) with 0.05% Tween-80 and 10% OADC enrichment (BD Biosciences) were grown to midlogarithmic phase at OD_{600} of ~0.6. Macrophages were seeded in six-well plates at a density of 5.0×10^5 cells per well and precultured in DMEM medium supplemented with 10% FBS for 12 hours before infection. Mtb were collected and washed twice in 1× phosphate-buffered saline (PBS) containing 0.05% Tween-80 and were then pelleted and thoroughly resuspended using DMEM medium with 0.05% Tween-80. Macrophages were then infected with Mtb strains at a multiplicity of infection (MOI) of 5 for 1 hour at 37°C to allow bacterial entry into cells. Thereafter, the culture media were discarded, and the cells were washed three times with 1× PBS to exclude noninternalized bacteria and were then incubated again with the fresh medium. At each designated time point, the cells and culture supernatants were collected for different analyses. To measure Mtb survival in macrophages, cells were lysed in 7H9 broth containing 0.05% SDS for 10 min. Bacterial colony-forming units (CFUs) were determined by serial-dilution plating on 7H10 agar plates, and the percent survival of Mtb was calculated by dividing the bacterial CFUs at the designated time point by that at time 0.

Cell transfection and retroviral transduction

Transient transfection of plasmid DNA in HEK293T cells or HeLa cells was carried out with Hieff Trans Liposomal Transfection Reagent (Yeasen) according to the manufacturer's instructions. To generate $Gsdmd^{-/-}$ iBMDMs stably expressing hGSDMD, the gene encoding hGSDMD was cloned into the retroviral plasmid pMSCVpuro. 293T cells were cotransfected with this retroviral construct and two packaging plasmids, pCMV-VSV-G and pCL-Eco, for 48 hours. The retroviral supernatant was then collected and filtered through a 0.45-μm filter and was used to transduce $Gsdmd^{-/-}$ iBMDMs in the presence of 4 μg/ml polybrene (Santa Cruz). Transduced cells were selected using 1 μg/ml puromycin (InvivoGen), and the expression of hGSDMD was verified by immunoblotting with anti-GSDMD antibody. For ex-

pression of exogenous PtpB or Lyn_{11}-FRB-GFP and GFP-FKBP-PJ in macrophages, in vitro transcribed mRNAs that encode these reconstituted proteins were transfected into the cells, as described previously (42, 43). Briefly, pCDNA6A and pCDNA6A-PtpB vectors were used to generate the linearized DNA templates for transcription of the control and $ptpB$ mRNAs, respectively, with a forward primer containing the T7 promotor sequence ahead of the start codon and a reverse primer located downstream of the stop codon; likewise, recombinant pEGFP-N1-Lyn_{11}-FRB and pEGFP-C1-FKBP-PJ vectors were used to generate the DNA templates for Lyn_{11}-FRB-GFP and GFP-FKBP-PJ, respectively (see table S1 for primers). The indicated mRNAs were then generated in vitro using the HiScribe T7 ARCA mRNA Kit (New England BioLabs, Cat# E2060), with incorporation of the modified nucleosides 5-methyl-CTP and pseudo-UTP (APExBIO, Cat# B7972 and B7967, respectively) to minimize the immunogenicity and enhance the stability (44). The transcribed mRNA was then dephosphorylated by Antarctic phosphatase (New England BioLabs, Cat# M0289) to avoid recognition by the cytoplasmic RNA sensors in macrophages (45, 46). Finally, the transcribed mRNA was purified using MEGAclear Transcription Clean-Up Kit (Thermo Fisher Scientific, Cat# AM1908). The purified mRNA was then transfected into BMDMs cultured in 6-well plates (500 ng for a total of 2.5×10^5 cells per well) using jetMESSENGER (Polyplus-transfection, Cat# 101000056) in accordance with the manufacturer's instructions. After transfection for 8 hours, the expression of the indicated proteins was verified by immunoblotting with anti-PtpB or anti-GFP antibodies or was examined by confocal microscopy.

Immunoblotting analysis and immunoprecipitation

Cells were lysed in the Cell Lysis Buffer for Western and Immunoprecipitation (IP) (Beyotime) or Radioimmunoprecipitation Assay (RIPA) Lysis Buffer (Beyotime) supplemented with 1 mM phenylmethanesulfonyl fluoride (PMSF). Proteins were separated by SDS–polyacrylamide gel electrophoresis (SDS-PAGE) and transferred to polyvinylidene difluoride membranes (Millipore). The membranes were blocked with 5% skimmed milk powder in tris-buffered saline with 0.1% Tween-20 (TBST) for 1 hour at room temperature (RT) and subsequently incubated with primary antibodies overnight at 4°C. The membranes were then incubated with goat anti-mouse IgG or goat anti-rabbit IgG conjugated to horseradish peroxidase (HRP) for 1 hour at RT after three washes of 10 min each with TBST. Finally, the membranes were developed by Immobilon Western Chemiluminescent HRP Substrate (Millipore) after three washes with TBST and exposed to x-ray film.

For immunoprecipitation, cells were lysed in a lysis buffer containing 50 mM Tris-HCl

(pH 7.4), 150 mM NaCl, 1 mM ethylenediaminetetraacetic acid (EDTA), 1% Triton X-100, and 1% protease inhibitor cocktail (Bimake). Cell lysates were incubated with Monoclonal Anti-HA Agarose (Sigma-Aldrich) for immunoprecipitation of HA-tagged protein in a vertical rotator at 4°C for 4 hours. After five washes with lysis buffer, the immunocomplexes bound in affinity beads were analyzed by SDS-PAGE and blotted with indicated antibodies.

Protein purification

E. coli BL21 (DE3) strain was used for bacterial expression of GST-fused Mtb PtpA and PtpB and its mutants (using pGEX-6P-1 vector), and of His$_6$-tagged NEDD8, ATG12, and Ub and its mutant (using pET30a vector). The bacterial strains were grown in LB medium at 37°C until OD$_{600}$ = 0.6. For GST-PtpB, GST-PtpA, His$_6$-Ub, and their mutants, isopropyl-β-D-thiogalactopyranoside (IPTG) was subsequently added to a final concentration of 400 μM, and cultures were shaken for further growing at 16°C for 16 hours. For His$_6$-tagged NEDD8 and ATG12, IPTG was used at 600 μM, and the cultures were shaken at 37°C for 4 hours. Cells were then harvested by centrifugation at 6,500*g* for 10 min and suspended in a buffer containing 20 mM Tris-HCl (pH 7.5) and 150 mM NaCl for cell-breaking with using Low-temperature Ultra-high Pressure Continuous Flow Cell Disrupters (JNBIO) or an Ultrasonic Homogenizer (Scientz Biotechnology). Glutathione Sepharose 4B (GE Healthcare) and Nickel Nitrilotriacetic Acid Agarose (Qiagen) were used, respectively, for purification of GST-fused proteins or His$_6$-tagged proteins by means of affinity chromatography, followed by size exclusion chromatography on a Superose 6 Increase 10/300 GL column (GE Healthcare).

In vitro precipitation assay

For the precipitation assay, 10 μg of GST or GST-protein fusions were immobilized onto 20 μl of Glutathione Sepharose 4B resins in 1 ml binding buffer (50 mM Tris, pH 7.5, 150 mM NaCl, 5 mM dithiothreitol, and 0.1% NP-40) supplemented with 1% protease inhibitor cocktail for 1 hour at 4°C. The resins were then washed three times with binding buffer and incubated with 10 μg of purified His$_6$-Ub, His$_6$-Ub (I44A), K48-linked poly-Ub (Ub$_4$), K63-linked poly-Ub (Ub$_4$), or M1-linked poly-Ub (Ub$_4$) in 1 ml binding buffer supplemented with 0.1 mg/ml bovine serum albumin (BSA). For analysis of the interactions between PtpB and Ub-like proteins (including NEDD8, FAT10, ISG15, SUMO1, UFM1, ATG12, ATG8, and URM1), GST-PtpB and His$_6$-tagged Ub (as control) or Ub-like proteins were used at 0.3 and 0.6 μM, respectively. Except that NEDD8 and ATG12 were expressed and purified from *E. coli* (as described above), His$_6$-tagged recombinant Ub-like proteins in-

cluding human FAT10 (Cat# ab113594), ISG15 (Cat# ab268685), SUMO1 (Cat# ab140417), UFM1 (Cat# ab104461), and URM1 (Cat# ab105598) were purchased from Abcam, and ATG8 (Cat# 14549-H07E) was purchased from Sino Biological. After 4 hours of incubation at 4°C, beads were extensively washed, and the bound protein complexes were subjected to SDS-PAGE and blotted with indicated antibodies.

Immunofluorescence microscopy

Alexa Fluor (488, 594, or 350) succinimidyl esters (Invitrogen) were used for Mtb staining before infection, as described previously (*47*). HeLa cells or macrophages were seeded on poly-lysine–coated coverslips and transfected or infected, as described above. For cell membrane staining, cells were gently washed with Hank's balanced salt solution (HBSS; Beyotime), and 50 μg/ml CF350-conjugated wheat germ agglutinin (Biotium) was applied to the cells on ice for 5 min in HBSS. Cells were then washed three times in HBSS and fixed in 4% paraformaldehyde (PFA) for 15 min at RT. Thereafter, cells were washed in 1× PBS and permeabilized with 0.5% Triton X-100 for 5 min. After three washes, the cells were blocked with 2% BSA for 30 min, subsequently incubated in indicated primary antibodies (anti-ASC: 1:400; anti-Flag: 1:400; anti-PtpA: 1:200; anti-PtpB: 1:800) diluted in 2% BSA for 1 hour. Cells were then washed in 1× PBS again and incubated with Alexa Fluor 594 or fluorescein isothiocyanate (FITC)–labeled secondary antibody (1:200; ZSGB-BIO) for another hour. After successive washing with 1× PBS and deionized water, the coverslips were mounted onto glass slides using 4',6-diamidino-2-phenylindole (DAPI) Staining Solution (Beyotime). Confocal images were taken with Olympus FV1000 confocal microscope and analyzed by FV10-ASW 4.2 (Olympus; https://www.olympus-global.com/).

For live-cell imaging, cells were plated in 20-mm glass-bottom dishes (NEST), which were placed in a humidified chamber supplemented with 5% CO$_2$ at 37°C during imaging. Images were acquired on an Olympus FV3000RS confocal laser scanning microscope equipped with a 60× silicone oil objective and were analyzed by FV31S-SW 2.3.1.163 (Olympus; https://www.olympus-global.com/).

Proximity ligation in situ assay

Proximity ligation assay (PLA) was performed using Duolink In Situ Detection Reagents Red (Sigma-Aldrich, Cat# DUO92008) according to Duolink PLA Fluorescence Protocol provided by the manufacturers. Briefly, ~1 × 10^5 BMDM cells were seeded on poly-lysine–coated coverslips and were infected with the indicated Mtb strains stained with Alexa Fluor 488 succinimidyl esters at a MOI of 5 for 24 hours. Cells were then washed, fixed, and permeabilized,

as described above, and blocked with Duolink Blocking Solution for 1 hour at 37°C. Thereafter, cells were incubated with mouse anti-mCaspase-1 antibody (diluted at 1:400) and rabbit anti-mASC (diluted at 1:400) or anti-Mtb (diluted at 1:800) antibody, in the Duolink Antibody Diluent for 1 hour at 37°C. For controls that determine the specificity of PLA, the anti-mCaspase-1 antibody was replaced by Mouse IgG1 Isotype Control (AdipoGen; Cat# AG-35B-0003PF), or the anti-mASC or anti-Mtb antibody was replaced by Normal Rabbit IgG (Cell Signaling Technology, Cat# 2729). After two washes, cells were further incubated with Duolink In Situ PLA probes (Anti-Mouse PLUS and Anti-Rabbit MINUS; Sigma-Aldrich, Cat# DUO92001 and DUO92005, respectively) diluted at 1:5 in the Duolink Antibody Diluent for another 1 hour at 37°C, allowing hybridization of PLA probes only if they were in close proximity (<40 nm). After two washes, cells were then incubated with a DNA ligase diluted at 1:50 in the Ligation Buffer for 30 min at 37°C. Next, cells were washed twice and incubated with a DNA polymerase at a 1:80 dilution in the Amplification Buffer for 90 min at 37°C. Finally, the coverslips were mounted onto glass slides using Duolink PLA Mounting Medium with DAPI and were subjected to confocal microscopy.

Plasma membrane and internal membrane staining

Immunocytochemistry for detection of PM PI4P and GSDMD-N was performed as previously described in detail (*19*). Briefly, cells were plated on poly-lysine–coated coverslips (for microscopy analysis) or collected in a 1.5-ml Eppendorf tube (for flow cytometer) and were fixed by 1× PBS containing 4% formaldehyde (FA) and 0.2% glutaraldehyde for 15 min at RT. After rinsing three times with 1× PBS containing 50 mM NH$_4$Cl, cells were chilled on ice for 5 min. Cells were then blocked and permeabilized with a piperazine-N,N'-bis(2-ethanesulfonic acid) (PIPES)–buffered saline (20 mM PIPES, pH 6.8, 137 mM NaCl, 2.7 mM KCl, 50 mM NH$_4$Cl) containing 5% normal goat serum (NGS; Yeasen) and 0.5% saponin (Sigma-Aldrich) on ice for 45 min. Primary antibodies (anti-PI4P: 1:200; anti-GSDMD-N: 1:100) were applied in PIPES-buffered saline with 5% NGS and 0.1% saponin on ice for 1 hour. Cells were then washed thrice in PIPES-buffered saline followed by incubation with Alexa Fluor 594 secondary antibody (1:200; ZSGB-BIO) in PIPES-buffered saline containing 5% NGS and 0.1% saponin on ice for 45 min. Cells were then rinsed four times with PIPES-buffered saline and were postfixed for 10 min on ice and 5 min at RT with 2% FA in 1× PBS. Thereafter, cells were washed thrice in 1× PBS containing 50 mM NH$_4$Cl and rinsed once in distilled water. Cells were then stained with DAPI for microscopy

analysis, as described above, or were resuspended in 1× PBS for flow cytometer analysis on a Fortessa flow cytometer (BD Biosciences). For IM PI4P staining, all steps were performed at RT, and a similar protocol was used, except that cells were fixed with 2% FA, and saponin was omitted, with the cells instead permeabilized with 20 μM digitonin (Abcam) for 5 min before staining (*19*).

Quantitative image analysis

For measurement of PM localization of PtpA or PtpB, the colocalizations of WGA with PtpA or PtpB were measured with FV10-ASW 4.0 (Olympus). Briefly, a line was drawn along the boundary of the cell to fully surround the cell. Then, the integrated intensity of each channel of interest and the Pearson's correlation coefficient between the channels of interest were determined. The fluorescence intensity of each fluorescent protein or lipid of interest was determined using the drawing/selection tool with the same software. Data are shown as mean ± SEM of at least four biological replicates, and ~100 cells were examined for each biological replicate. Results are representative of at least three independent experiments.

Intracellular potassium measurement

BMDM cells were seeded on poly-lysine–coated coverslips and infected with or without Mtb strains at a MOI of 5. At 48 hours after infection, medium was replaced with FBS-free DMEM containing 10 μM of Enhanced Potassium Green-2 (EPG-2) AM (Shanghai Maokang Biotechnology), which is a potassium-specific probe, and 0.5% (w/v) pluronic acid F-127, which aids in efficient permeation of EPG-2 AM into the cells. After 1 hour of incubation at 37°C, cells were extensively washed with 1× PBS followed by immunofluorescence microscopy analysis using anti-Mtb antibody. For fluorescence measurement, BMDM cells were plated in 96-well clear bottom black plates and were infected with Mtb strains as described above. After incubation with EPG-2 AM, the fluorescence was determined with a Cytation 5 Plate Reader (BioTek, USA).

Cell membrane integrity assay

BMDM cells were seeded on poly-lysine–coated coverslips and infected with or without Mtb strains pre-stained with Alexa Fluor 488 succinimidyl ester at a MOI of 5. At 48 hours after infection, 15 μM of propidium iodide (PI; Beyotime) was added to the medium for monitoring cell membrane integrity. After 20 min of incubation at 37°C, cells were washed with 1× PBS thrice followed by immunofluorescence microscopy analysis as described above. Approximately 100 cells were examined for quantitative analysis of PI-positive cells, and results are represented as mean ± SEM from four independent experiments.

Cell fractionation assay

For separation of the cytosol and PM fractions of BMDMs, cells were seeded in 10-cm plates and infected with indicated Mtb strains for 48 hours as described above. Approximately $2 × 10^7$ cells were then harvested for separation of total cellular components into different fractions with Minute Plasma Membrane Protein Isolation and Cell Fractionation Kit (Invent Biotechnologies) according to the manufacturers' instructions. Finally, the cytosol and PM fractions were collected, and ~100 μg cytosolic and PM proteins were separately dissolved in 100 μl SDS sample buffer for analysis by SDS-PAGE and blotted with indicated antibodies.

For separation of the bacterial and macrophage cytosolic fractions of Mtb-infected BMDMs, cells were lysed in hypotonic lysis buffer (containing 10 mM HEPES, pH 7.9, 1.5 mM $MgCl_2$, 10 mM KCl, 0.34 M sucrose, 10% glycerol, 0.1% Triton X-100, and 1% protease inhibitor cocktail) as described previously (*5*). The lysis mixture was then centrifuged at 4°C, 1300*g* for 10 min to pellet the bacteria with macrophage nuclei. The supernatant was collected as the cytosolic fraction of macrophages. The bacteria (with macrophage nuclei) and macrophage cytosolic fraction were dissolved in SDS sample buffer for analysis by SDS-PAGE and blotted with indicated antibodies.

Enzyme-linked immunosorbent assay and cell cytotoxicity analysis

Cell culture media, mouse bronchoalveolar lavage fluid (BALF), or cell-free supernatants from mouse lung homogenates were collected for quantitative detection of cytokines including IL-1β, IL-18, TNF-α, IL-6, IL-12 (p40), IL-10, or IFN-γ with commercial ELISA kits according to the manufacturers' instructions. Human and mouse IL-1β ELISA kits and mouse IL-18, TNF-α, IL-6, IL-12 (p40), and IL-10 ELISA kits were purchased from RayBiotech, and mouse IFN-γ ELISA kit was purchased from Cloud-Clone Corp.

Quantitative analysis of cellular phosphoinositides

To determine the concentrations of PM- and IM-derived PI4P and PI(4,5)P₂ from BMDMs, ~2 × 10^7 cells were collected for cell fractionation to obtain the PM and IM fractions using Minute Plasma Membrane Protein Isolation and Cell Fractionation Kit (Invent Biotechnologies). The separated membrane fractions were then resuspended in ice-cold 0.5 M trichloroacetic acid (TCA) in conical glass centrifuge tubes (Kimble) and incubated on ice for 5 min, followed by centrifugation at 1500*g* for 7 min at 4°C. The pellet was then washed two times with 5% TCA containing 1 mM EDTA at RT and was resuspended in MeOH:CHCl₃ (2:1)

with 10-min vortex to extract neutral lipids (twice). The supernatant (containing neutral lipids) was discarded after centrifugation at 1500*g* for 5 min at RT, and the pellet was resuspended in 750 μl MeOH:CHCl₃:HCl (80:40:1) with 25-min vortex to extract acidic lipids. The supernatant (containing acidic lipids) was then collected after centrifugation at 1500*g* for 5 min at RT and was mixed with 250 μl of CHCl₃ and 450 μl of 0.1 M HCl. After 30-s vortex, the mixture was centrifuged at 1500*g* for 5 min at RT, and the organic (lower) phase was collected into the screw-cap glass vials (Thermo Fisher Scientific) and was dried in a vacuum dryer. The dried lipid abstracts were stored at −80°C until use, or immediately reconstituted in relevant detecting buffer with sonication for 10 min at RT using a water bath sonicator, and were then subjected to quantitative detection of PI4P and PI(4,5)P₂ using PI4P and PI(4,5)P₂ Mass ELISA Assay Kits (Echelon Biosciences), respectively, according to the manufacturers' instructions.

Quantitative PCR analysis

Mtb-infected macrophages or mouse lung homogenates were used for total RNA extraction with RNeasy Plus Mini Kit according the manufacturers' instructions (Qiagen). The reverse transcription of RNA was accomplished by using a 1st Strand cDNA Synthesis Kit (Yeasen) and performed to quantitative PCR (qPCR) analysis with Hieff qPCR SYBR Green Master Mix (Yeasen) on ABI 7500 system (Applied Biosystems). Quantitative expression of targeted gene was normalized to *Gapdh*. All qPCR primers are listed in table S1.

Protein-liposome binding assay

Liposomes were prepared as previously described (*10*). Briefly, phosphatidylcholine (PC; Avanti Polar Lipids, Cat# 850457), phosphatidylinositol (Avanti Polar Lipids, Cat# 850149), PI4P (Avanti Polar Lipids, Cat# 840045), and PI(4,5)P₂ (Avanti Polar Lipids, Cat# 850155) were dissolved in MeOH:CHCl₃ (20:9). Thereafter, 0.4 μmol of PC was mixed with 0.1 μmol of phosphatidylinositol, PI4P, or PI(4,5)P₂ in the screw-cap glass vials (Thermo Fisher Scientific), and the mixture was dried in a vacuum dryer. The dried lipids were then reconstituted in 500 μl binding buffer (20 mM HEPES, pH 7.5 and 150 mM NaCl). Liposomes were produced by extrusion of the hydrated lipids through a 0.1-μm polycarbonate filter 35 times using the Mini-Extruder device (Avanti Polar Lipids). For liposome-binding assay, purified GST-fused PtpB or its mutants (0.5 μM) were incubated with the indicated liposomes (containing 0.5 mM lipids) at RT for 1 hour in a total volume of 100 μl. The mixtures were then centrifuged at 100,000*g* for 20 min at 4°C in a Beckman Optima MAX-XP ultracentrifuge. The liposome-free supernatant was collected, and

the liposome pellets were further washed twice with 100 μl binding buffer by re-centrifugation before collection. The supernatant and pellet fractions were then analyzed by SDS-PAGE and blotted using anti-GST antibody.

Protein-lipid binding assay

GST or GST-fused PtpB proteins were spotted on PIP strips or membrane lipid strips (Echelon Biosciences) according to the manufacturer's instructions. Briefly, lipid strips were blocked with 1× PBS containing 0.1% Tween-20 (PBST) and 3% fatty acid–free bovine serum albumin (BSA; Biotopped) for 1 hour at RT. The strips were then incubated with 2 μg/ml protein diluted in PBST buffer containing 3% BSA for 1 hour at RT, followed by three washes with PBST buffer. Membrane-bound proteins were detected by incubating the lipid strips with anti-GST-tag HRP-DirecT antibody (MBL International) diluted 1: 2000 in PBST buffer containing 3% BSA for 1 hour at RT. After washing three times with PBST buffer, proteins were visualized using Immobilon Western Chemiluminescent HRP Substrate (Millipore) and exposed to x-ray film.

Intracellular delivery of phosphoinositides

Shuttle PIP Kits purchased from Echelon Biosciences were used for intracellular delivery of phosphoinositides according to their protocols. In brief, 2×10^5 BMDM cells were cultured in 500 μl DMEM with 10% FBS in 24-well plates and infected with or without Mtb strains for 1 hour as described above. Phosphoinositides and polyamine carriers were reconstituted in DMEM and combined with a ratio of 1:1 (100 μM final concentration each) for 10 min at RT. Then the mixtures were diluted with DMEM and were used for incubation of cells for 4 hours at 37°C. The final phosphoinositide and carrier concentrations on cells were both 10 μM. For the negative control, cells were treated with carriers only according to this procedure. After treatment, the culture media were discarded, and the cells were incubated again with the fresh medium. At 24 hours after infection, the cells and supernatants were collected for CFU counting, cell cytotoxicity assay, or ELISA. The exogenous phosphoinositide uptake efficiency of cells was verified by flow cytometer analysis on FACS Calibur (BD Biosciences) using fluorescent phosphoinositides labeled with the green fluorophore BODIPY-FL (Echelon Biosciences) for intracellular delivery according to the same protocol.

Phosphatase activity assay and kinetic determination

Malachite Green Phosphate Detection Kit (Cell Signaling Technology) was used for quantitation of free phosphate during the dephosphorylation of phosphoinositide according to

the manufacturer's protocol. The PI4P phosphatase activity assay was carried out using a 50 μl reaction mixture containing reaction buffer (20 mM Tris-Base, pH 7.4, 150 mM NaCl and 1 mM EDTA), 80 μM of diC16-PI4P (Echelon Biosciences), and various concentrations (0.01 to 2 μM) of purified proteins (GST, GST-fused PtpB or PtpB mutants). The reaction mixtures were incubated at 37°C for 15 min before the addition of 50 μl of Malachite Green Reagent. After further incubation for 30 min at RT, the absorbance was measured at 630 nm on a spectrophotometer. Control reactions containing no proteins were included to measure the background level of phosphate. The concentration of released inorganic phosphate was determined using a phosphate standard curve created with Phosphate Standard. For kinetic analysis, the initial dephosphorylation rate (V_0) of each phosphoinositide catalyzed by PtpB or its mutants (0.5 μM each) was determined from reactions with various concentrations (0 to 200 μM) of PI3P, PI4P, PI5P, PI(3,4)P$_2$, PI(3,5)P$_2$, PI(4,5)P$_2$, and PI(3,4,5)P$_3$ (Echelon Biosciences) in the presence or absence of His$_6$-Ub (0.5 μM) according to the same procedure. Similarly, the V_0 of protein substrates catalyzed by PtpB or its mutants (0.5 μM each) was determined using 0 to 1000 μM of phosphotyrosine peptides, pTyr-EGFR and pTyr-IGF1R. The Lineweaver-Burk plots were used to determine the Michaelis-Menten kinetic parameters (k_{cat} and K_m).

Mouse infection

For in vivo Mtb H37Rv infection, 6- to 8-weeks-old female mice were infected via the aerosol route using an inhalation exposure system (Glas-Col Inc.) as previously described (48). Briefly, log-phase Mtb cultures were washed twice with 1× PBS and were sonicated to generate single cell suspension. Bacteria were then resuspended in 10 ml 1× PBS at an OD_{600} of 0.1, and 5 ml of this inoculum was loaded into the inhalation exposure nebulizer. The aerosol unit was programmed to deliver ~100 CFUs per animal, as determined by plating whole lung homogenates from five mice on Middlebrook 7H10 agar for CFU counting within 24 hours of infection. At each designated time point, lungs were homogenized with a FastPrep-24 System (MP Biomedicals) for ELISA, qPCR analysis, or CFU counting or subjected to section along with livers for further analysis. BALF was obtained by washing the lung airways with 1 ml 1× PBS per mouse according to a previously detailed protocol (49), and after centrifugation, the cell-free supernatants were assayed by ELISA. All animal studies were approved by the Biomedical Research Ethics Committee of Institute of Microbiology (Chinese Academy of Sciences).

Histopathology and tissue immunofluorescence

Lungs or livers from Mtb-infected or control mice were fixed by inflating the tissues with 4% formaldehyde, sectioned, and stained with hematoxylin and eosin or by the Ziehl-Neelsen method to visualize acid-fast mycobacteria. Slides containing histological sections were scanned with Aperio CS2 (Leica Biosystems), and quantitation of the inflammation area in each tissue section was performed using ImageJ 1.50e with an IHC Toolbox plugin (National Institutes of Health; https://imagej.nih.gov/ij/). For lung immunofluorescence analysis, Mtb was detected using anti-Mtb antibody (1:200) with a Two-step IHC Detection Kit (ZSGB-BIO), followed by amplification with tyramide (1:200) using Opal 570 Reagent Pack (AKOYA) according to the manufacturer's instructions. Slides were then rinsed three times with 1× PBS and were subjected to TUNEL assay using One-step TUNEL Assay Kit (KeyGEN BioTECH) according to the manufacturer's protocol. DAPI Staining Solution (Beyotime) was used to visualize the nuclei and to mount the slides. Slides were scanned using Aperio Versa 200 (Leica Biosystems) and quantitation of the TUNEL$^+$ cells in each lung section was performed using Imaris 9.6 (Bitplane; https://imaris.oxinst.com/).

Structure analysis

The structure information of PtpB and Ub was retrieved from Protein Data Bank (PDB IDs 1YWF and 1UBQ, respectively; https://www.rcsb.org/). Multiple sequence alignments were performed using MUSCLE (50). The secondary structure of PtpB 3E mutant was predicted using the SOPMA algorithm (https://npsa-prabi.ibcp.fr/) or AlphaFold2 (https://github.com/deepmind/alphafold) (51, 52). All structural figures were generated in PyMOL (http://www.pymol.org).

Statistics

Two-way analysis of variance (ANOVA) was used for analysis of experiments with multiple groups and multiple independent variables, and one-way ANOVA was used for analysis of multiple groups with a single independent variable. The Tukey and Dunnett tests were used as follow-up tests to the ANOVAs, where the Tukey test was used to compare every mean with every other mean, and the Dunnett test was used when comparing every mean to a control mean. Unpaired two-tailed Student's t tests were used for single comparison of two groups. The quantified data with statistical analysis were performed using GraphPad Prism 8.0 (https://www.graphpad.com/). $P > 0.05$, not significant (ns); *$P < 0.05$; **$P < 0.01$; ***$P < 0.001$; ****$P < 0.0001$. Data are shown as mean ± SEM of at least three biological replicates, and results are representative of at least three independent experiments unless otherwise designated in figure legends.

REFERENCES AND NOTES

1. S. Bagcchi, Dismal global tuberculosis situation due to COVID-19. *Lancet Infect. Dis.* **21**, 1636 (2021). doi: 10.1016/S1473-3099(21)00713-1; pmid: 34838229

2. J. P. Ernest *et al*., Development of new tuberculosis drugs:Translation to regimen composition for drug-sensitive and multidrug-resistant tuberculosis. *Annu. Rev. Pharmacol. Toxicol.* **61**, 495–516 (2021). doi: 10.1146/annurev-pharmtox-030920-011143; pmid: 32806997

3. M. A. Forrellad *et al*., Virulence factors of the *Mycobacterium tuberculosis* complex. *Virulence* **4**, 3–66 (2013). doi: 10.4161/viru.22329; pmid: 23076359

4. Q. Chai, L. Wang, C. H. Liu, B. Ge, New insights into the evasion of host innate immunity by *Mycobacterium tuberculosis*. *Cell. Mol. Immunol.* **17**, 901–913 (2020). doi: 10.1038/s41423-020-0502-z; pmid: 32728204

5. J. Wang *et al*., *Mycobacterium tuberculosis* suppresses innate immunity by coopting the host ubiquitin system. *Nat. Immunol.* **16**, 237–245 (2015). doi: 10.1038/ni.3096; pmid: 25642820

6. S. M. Man, T. D. Kanneganti, Regulation of inflammasome activation. *Immunol. Rev.* **265**, 6–21 (2015). doi: 10.1111/imr.12296; pmid: 25879280

7. D. E. Place, T. D. Kanneganti, Recent advances in inflammasome biology. *Curr. Opin. Immunol.* **50**, 32–38 (2018). doi: 10.1016/j.coi.2017.10.011; pmid: 29128729

8. R. Kang *et al*., Lipid peroxidation drives gasdermin D-mediated pyroptosis in lethal polymicrobial sepsis. *Cell Host Microbe* **24**, 97–108.e4 (2018). doi: 10.1016/j.chom.2018.05.009; pmid: 29937272

9. X. Chen *et al*., Pyroptosis is driven by non-selective gasdermin-D pore and its morphology is different from MLKL channel-mediated necroptosis. *Cell Res.* **26**, 1007–1020 (2016). doi: 10.1038/cr.2016.100; pmid: 27573174

10. J. Ding *et al*., Pore-forming activity and structural autoinhibition of the gasdermin family. *Nature* **535**, 111–116 (2016). doi: 10.1038/nature18590; pmid: 27281216

11. T. K. Phan, G. K. Bindra, S. A. Williams, I. K. H. Poon, M. D. Hulett, Combating human pathogens and cancer by targeting phosphoinositides and their metabolism. *Trends Pharmacol. Sci.* **40**, 866–882 (2019). doi: 10.1016/j.tips.2019.09.006; pmid: 31677918

12. K. Wang *et al*., Structural mechanism for GSDMD targeting by autoprocessed caspases in pyroptosis. *Cell* **180**, 941–955.e20 (2020). doi: 10.1016/j.cell.2020.02.002; pmid: 32109412

13. I. Banerjee *et al*., Gasdermin D restrains type I interferon response to cytosolic DNA by disrupting ionic homeostasis. *Immunity* **49**, 413–426.e5 (2018). doi: 10.1016/j.immuni.2018.07.006; pmid: 30170814

14. B. Zhou *et al*., Targeting mycobacterium protein tyrosine phosphatase B for antituberculosis agents. *Proc. Natl. Acad. Sci. U.S.A.* **107**, 4573–4578 (2010). doi: 10.1073/pnas.0909133107; pmid: 20167798

15. L. Fan *et al*., MptpB promotes mycobacteria survival by inhibiting the expression of inflammatory mediators and cell apoptosis in macrophages. *Front. Cell. Infect. Microbiol.* **8**, 171 (2018). doi: 10.3389/fcimb.2018.00171; pmid: 29888212

16. N. Beresford *et al*., MptpB, a virulence factor from *Mycobacterium tuberculosis*, exhibits triple-specificity phosphatase activity. *Biochem. J.* **406**, 13–18 (2007). doi: 10.1042/BJ20070670; pmid: 17584180

17. A. Koul *et al*., Cloning and characterization of secretory tyrosine phosphatases of *Mycobacterium tuberculosis*. *J. Bacteriol.* **182**, 5425–5432 (2000). doi: 10.1128/JB.182.19.5425-5432.2000; pmid: 10986245

18. J. Wang *et al*., The mycobacterial phosphatase PtpA regulates the expression of host genes and promotes cell proliferation. *Nat. Commun.* **8**, 244 (2017). doi: 10.1038/s41467-017-00279-z; pmid: 28811474

19. G. R. Hammond, G. Schiavo, R. F. Irvine, Immunocytochemical techniques reveal multiple, distinct cellular pools of PtdIns4P and PtdIns(4,5)P₂. *Biochem. J.* **422**, 23–35 (2009). doi: 10.1042/BJ20090428; pmid: 19508231

20. X. Li *et al*., A genetically encoded fluorescent probe to visualize intracellular phosphatidylinositol 3,5-bisphosphate localization and dynamics. *Proc. Natl. Acad. Sci. U.S.A.* **110**, 21165–21170 (2013). doi: 10.1073/pnas.1311864110; pmid: 24324172

21. N. Vashi, S. B. Andrabi, S. Ghanwat, M. Suar, D. Kumar, Ca²⁺-dependent focal exocytosis of Golgi-derived vesicles helps phagocytic uptake in macrophages. *J. Biol. Chem.* **292**, 5144–5165 (2017). doi: 10.1074/jbc.M116.743047; pmid: 28174296

22. T. Welz, J. Wellbourne-Wood, E. Kerkhoff, Orchestration of cell surface proteins by Rab11. *Trends Cell Biol.* **24**, 407–415 (2014). doi: 10.1016/j.tcb.2014.02.004; pmid: 24675420

23. G. R. Hammond *et al*., PI4P and PI(4,5)P₂ are essential but independent lipid determinants of membrane identity. *Science* **337**, 727–730 (2012). doi: 10.1126/science.1222483; pmid: 22722250

24. I. Vergne *et al*., Mechanism of phagolysosome biogenesis block by viable *Mycobacterium tuberculosis*. *Proc. Natl. Acad. Sci. U.S.A.* **102**, 4033–4038 (2005). doi: 10.1073/pnas.0409716102; pmid: 15753315

25. C. Grundner, H. L. Ng, T. Alber, *Mycobacterium tuberculosis* protein tyrosine phosphatase PtpB structure reveals a diverged fold and a buried active site. *Structure* **13**, 1625–1634 (2005). doi: 10.1016/j.str.2005.07.017; pmid: 16271885

26. S. Hirano *et al*., Double-sided ubiquitin binding of Hrs-UIM in endosomal protein sorting. *Nat. Struct. Mol. Biol.* **13**, 272–277 (2006). doi: 10.1038/nsmb1051; pmid: 16462748

27. C. Huppertz *et al*., The NLRP3 inflammasome pathway is activated in sarcoidosis and involved in granuloma formation. *Eur. Respir. J.* **55**, 1900119 (2020). doi: 10.1183/13993003.00119-2019; pmid: 31949113

28. I. Jorgensen, E. A. Miao, Pyroptotic cell death defends against intracellular pathogens. *Immunol. Rev.* **265**, 130–142 (2015). doi: 10.1111/imr.12287; pmid: 25879289

29. Q. Chai, Y. Zhang, C. H. Liu, *Mycobacterium tuberculosis*: An adaptable pathogen associated with multiple human diseases. *Front. Cell. Infect. Microbiol.* **8**, 158 (2018). doi: 10.3389/fcimb.2018.00158; pmid: 29868514

30. S. Gagneux, Ecology and evolution of *Mycobacterium tuberculosis*. *Nat. Rev. Microbiol.* **16**, 202–213 (2018). doi: 10.1038/nrmicro.2018.8; pmid: 29456241

31. Y. Liu *et al*., Gasdermin E-mediated target cell pyroptosis by CAR T cells triggers cytokine release syndrome. *Sci. Immunol.* **5**, eaax7969 (2020). doi: 10.1126/sciimmunol.aax7969; pmid: 31953257

32. Z. Zheng *et al*., The lysosomal Rag-Ragulator complex licenses RIPK1− and caspase-8−mediated pyroptosis by *Yersinia*. *Science* **372**, eabg0269 (2021). doi: 10.1126/science.abg0269; pmid: 35058659

33. Y. Wang *et al*., Chemotherapy drugs induce pyroptosis through caspase-3 cleavage of a gasdermin. *Nature* **547**, 99–103 (2017). doi: 10.1038/nature22393; pmid: 28459430

34. G. Luchetti *et al*., Shigella ubiquitin ligase IpaH7.8 targets gasdermin D for degradation to prevent pyroptosis and enable infection. *Cell Host Microbe* **29**, 1521–1530.e10 (2021). doi: 10.1016/j.chom.2021.08.010; pmid: 34492225

35. A. Ahmed *et al*., A century of BCG: Impact on tuberculosis control and beyond. *Immunol. Rev.* **301**, 98–121 (2021). doi: 10.1111/imr.12968; pmid: 33955564

36. M. Ouimet *et al*., *Mycobacterium tuberculosis* induces the miR-33 locus to reprogram autophagy and host lipid metabolism. *Nat. Immunol.* **17**, 677–686 (2016). doi: 10.1038/ni.3434; pmid: 27089382

37. J. Daniel, H. Maamar, C. Deb, T. D. Sirakova, P. E. Kolattukudy, *Mycobacterium tuberculosis* uses host triacylglycerol to accumulate lipid droplets and acquires a dormancy-like phenotype in lipid-loaded macrophages. *PLOS Pathog.* **7**, e1002093 (2011). doi: 10.1371/journal.ppat.1002093; pmid: 21731490

38. D. G. Russell, P. J. Cardona, M. J. Kim, S. Allain, F. Altare, Foamy macrophages and the progression of the human tuberculosis granuloma. *Nat. Immunol.* **10**, 943–948 (2009). doi: 10.1038/ni.1781; pmid: 19692995

39. H. Hu, S. C. Sun, Ubiquitin signaling in immune responses. *Cell Res.* **26**, 457–483 (2016). doi: 10.1038/cr.2016.40; pmid: 27012466

40. J. C. van Kessel, G. F. Hatfull, Recombineering in *Mycobacterium tuberculosis*. *Nat. Methods* **4**, 147–152 (2007). doi: 10.1038/nmeth996; pmid: 17179933

41. A. Balla *et al*., Maintenance of hormone-sensitive phosphoinositide pools in the plasma membrane requires phosphatidylinositol 4-kinase IIIα. *Mol. Biol. Cell* **19**, 711–721 (2008). doi: 10.1091/mbc.e07-07-0713; pmid: 18077555

42. M. Herb *et al*., Mitochondrial reactive oxygen species enable proinflammatory signaling through disulfide linkage of NEMO. *Sci. Signal.* **12**, eaar5926 (2019). doi: 10.1126/scisignal.aar5926; pmid: 30755476

43. H. Zhang *et al*., 5-Hydroxymethylfurfural alleviates inflammatory lung injury by inhibiting endoplasmic reticulum stress and NLRP3 inflammasome activation. *Front. Cell Dev. Biol.* **9**, 782427 (2021). doi: 10.3389/fcell.2021.782427; pmid: 34966742

44. M. S. Kormann *et al*., Expression of therapeutic proteins after delivery of chemically modified mRNA in mice. *Nat. Biotechnol.* **29**, 154–157 (2011). doi: 10.1038/nbt.1733; pmid: 21217696

45. V. Hornung *et al*., 5'-Triphosphate RNA is the ligand for RIG-I. *Science* **314**, 994–997 (2006). doi: 10.1126/science.1132505; pmid: 17038590

46. A. Pichlmair *et al*., RIG-I-mediated antiviral responses to single-stranded RNA bearing 5'-phosphates. *Science* **314**, 997–1001 (2006). doi: 10.1126/science.1132998; pmid: 17038589

47. Q. Chai *et al*., A *Mycobacterium tuberculosis* surface protein recruits ubiquitin to trigger host xenophagy. *Nat. Commun.* **10**, 1973 (2019). doi: 10.1038/s41467-019-09955-8; pmid: 31036822

48. A. J. Wolf *et al*., *Mycobacterium tuberculosis* infects dendritic cells with high frequency and impairs their function *in vivo*. *J. Immunol.* **179**, 2509–2519 (2007). doi: 10.4049/jimmunol.179.4.2509; pmid: 17675513

49. L. Van Hoecke, E. R. Job, X. Saelens, K. Roose, Bronchoalveolar lavage of murine lungs to analyze inflammatory cell infiltration. *J. Vis. Exp.* **2017**, e55398 (2017). doi: 10.3791/55398; pmid: 28518083

50. R. C. Edgar, MUSCLE: Multiple sequence alignment with high accuracy and high throughput. *Nucleic Acids Res.* **32**, 1792–1797 (2004). doi: 10.1093/nar/gkh340; pmid: 15034147

51. C. Geourjon, G. Deléage, SOPMA: Significant improvements in protein secondary structure prediction by consensus prediction from multiple alignments. *Comput. Appl. Biosci.* **11**, 681–684 (1995). doi: 10.1093/bioinformatics/11.6.681; pmid: 8808585

52. K. Tunyasuvunakool *et al*., Highly accurate protein structure prediction for the human proteome. *Nature* **596**, 590–596 (2021). doi: 10.1038/s41586-021-03828-1; pmid: 34293799

53. Q. Chai, A bacterial phospholipid phosphatase inhibits host pyroptosis by hijacking ubiquitin, version 1, Mendeley Data (2022); https://doi.org/10.17632/r53vh3tdmg.1.

54. LuShuYangMing, LuShuYangMing/Function_annotation_of_MTB_Genome: Function annotation of MTB genome, version 1.0.0, Zenodo (2022); https://doi.org/10.5281/zenodo.7021021.

Science

A bacterial phospholipid phosphatase inhibits host pyroptosis by hijacking ubiquitin

Qiyao ChaiShanshan YuYanzhao ZhongZhe LuChanggen QiuYang YuXinwen ZhangYong ZhangZehui LeiLihua QiangBing-Xi LiYu PangXiao-Bo QiuJing WangCui Hua Liu

How a pathogen inhibits pyroptosis

Pyroptosis is a proinflammatory form of programmed cell death adopted by mammalian hosts to control infections, but how pathogens evade this immune response remains largely unexplored. Chai *et al.* found that PtpB, a known protein phosphatase secreted by *Mycobacterium tuberculosis*, acts as a phospholipid phosphatase that dephosphorylates host plasma membrane phosphoinositides upon activation by ubiquitin to inhibit pyroptosis. These findings reveal a delicate strategy by which pathogens suppress pyroptosis by altering host membrane composition, and provide a potential tuberculosis treatment by targeting the PtpB-ubiquitin interacting interface. —SMH

View the article online
https://www.science.org/doi/10.1126/science.abq0132
Permissions
https://www.science.org/help/reprints-and-permissions

Use of this article is subject to the Terms of service